PERFORMANCE MEASUREMENTS
OF DIRECT AIR INJECTION IN A
CAVITY-BASED FLAMEHOLDER
FOR A SUPERSONIC COMBUSTOR

THESIS

Scott G. Edens

AFIT/GAE/ENY/06-02

DEPARTMENT OF THE AIR FORCE
AIR UNIVERSITY

AIR FORCE INSTITUTE OF TECHNOLOGY

Wright-Patterson Air Force Base, Ohio

AFIT/GAE/ENY/06-02

PERFORMANCE MEASUREMENTS OF DIRECT AIR INJECTION IN A CAVITY-BASED FLAMEHOLDER FOR A SUPERSONIC COMBUSTOR

THESIS

Presented to the Faculty

Department of Aeronautics and Astronautics

Graduate School of Engineering and Management

Air Force Institute of Technology

Air University

Air Education and Training Command

In Partial Fulfillment of the Requirements for the

Degree of Master of Science in Aeronautical Engineering

Scott G. Edens

December 2005

APPROVED FOR PUBLIC RELEASE; DISTRIBUTION UNLIMITED.

AFIT/GAE/ENY/06-02

PERFORMANCE MEASUREMENTS OF DIRECT AIR INJECTION IN A CAVITY-BASED FLAMEHOLDER FOR A SUPERSONIC COMBUSTOR

Scott G. Edens

Approved:

Paul I. King (Chairman)		date

Ralph A. Anthenien Jr. (Member)		date

Mark F. Reeder (Member)		date

AFIT/GAE/ENY/06-02

Abstract

For several years the Air Force Research Lab Propulsion Directorate has been studying

the difficulties in fueling supersonic combustion ramjet engines with hydrocarbon based

fuels. Recent investigations have focused on the use of direct air injection into a directly-

fueled cavity-based flameholder. Direct air injection has been shown qualitatively to be a

valuable tool for improving cavity combustion. Little quantitative data is available that

characterizes the performance of cavity-based flameholders. The objective of this

research was to quantitatively determine the specific advantages and disadvantages of the

direct air injection scheme. This was accomplished via intrusive probing into a

supersonic free stream flow at an axial location behind the cavity flameholder. Pitot and

static pressure, total temperature, and gas sampling measurements were taken and the

corresponding values were processed to yield relevant engineering quantities. Data were

taken over a range of fuel and air injection rates. Direct air injection resulted in increased

combustion throughout the area of interest behind the cavity. Air injection increased the

static temperature and pressure throughout the area of interest. Enthalpy spread into the

free stream was also increased through the use of air injection. Total pressure losses

increased as a result of the direct air injection scheme. The ratio of enthalpy increase to

increase in total pressure losses increased with higher fuel flow rates, indicating that the

direct air injection technique shows more promise for higher fuel loadings.

Acknowledgements

Table of Contents

List of Figures

Figure   Page

List of Tables

List of Symbols

A	Area
c_1	Sound speed ahead of shock
c_p	Constant pressure specific heat
C_xH_y	Generic hydrocarbon formula
CH_3	Methyl radical
d	Injection port diameter
D	Cavity depth
g	Gram
h	Pylon height
h_1	Flow enthalpy at inlet entrance
h_2	Flow enthalpy at combustor entrance
h_1	Enthalpy ahead of shock
h_t	Total enthalpy
in	Inch
u_1	Flow velocity at inlet entrance
u_2	Flow velocity at combustor entrance
l	Pylon axial length
L	Cavity length
M_1	Mach number
$\dot{m}_1$	Mass flow ahead of shock
NO_x	Nitrous oxide
O_2	Oxygen
$\dot{p}_1$	Momentum flow ahead of shock
psi	Pounds per square inch
psia	Pounds per square inch (absolute)
P_1	Static pressure ahead of shock
$P_{t,1}$	Total pressure ahead of shock
$P_{t,2}$	Pitot pressure measured by probe
P_c	Static pressure measured by cone probe
P_o	Total pressure
R_{gas}	Specific gas constant of gas
SLPM	Standard liters per minute
T_1	Flow temperature at inlet entrance
$T_{t,1}$	Total temperature ahead of probe shock
T_1	Static temperature ahead of probe shock
T_2	Flow temperature at combustor entrance

$T_{t,2}$	Total temperature behind probe shock
W	Pylon width
X-axis	Free stream direction
X_p	Distance from Pylon rear to injection port center
Y-axis	Vertical direction
Z-Axis	Spanwise direction
γ	Specific heat ratio
θ	Pylon angle
ρ_1	Static density ahead of shock
Φ	Equivalence ratio

PERFORMANCE MEASUREMENTS OF DIRECT AIR INJECTION IN A CAVITY-BASED FLAMEHOLDER FOR A SUPERSONIC COMBUSTOR

I. Introduction

Background:

The interest in hypersonic flight is obvious in that it serves as a logical step forward from lower supersonic speeds in increasing the performance of aerospace vehicles. Civil transports traveling at hypersonic speeds could make intercontinental flights in a few hours. For military applications, being able to project power anywhere in the world in a matter of hours is highly attractive. This could be accomplished with aircraft or missiles traveling at hypersonic speeds. An added benefit of the hypersonic velocity is that the kinetic energy associated with those speeds can serve as the destructive force in a missile or projectile. The need for a chemically explosive warhead could be eliminated, meaning that fewer chemical explosives would need to be purchased and stored safely.

Hypersonic velocities are difficult to achieve however. Few aircraft powered by conventional turbine or even ramjet engines have approached the hypersonic realm. The Lockheed SR-71 Blackbird and the XB-70 Valkyrie both flew in excess of Mach 3, but could not come close to achieving Mach 5. Until the recent flight tests conducted as part of the NASA X-43 program, all ventures into the hypersonic flight regime have employed the use of rockets, with the first manned hypersonic flights coming during the X-15 program. Rockets have the disadvantage of not just needing to carry their own oxidizer, but their own propulsive medium as well. Rockets use the fuel and oxidizer

necessary for combustion as the medium through which a propulsive force is applied. Air-breathing engines use the atmosphere as the propulsive medium, and thus have much higher specific impulses. The higher specific impulse of air-breathing engines allows for larger payload capacity and greater range for a given vehicle size, in comparison with vehicles powered by rocket engines. While unable to operate in the vacuum of space, an air-breathing hypersonic vehicle could serve as a launching platform for space missions. Air-breathing hypersonic platforms can serve as the first stage in a two-stage space launch system by providing an initial velocity and altitude gain for the space-fairing second stage.

The leading technology for the goal of air-breathing hypersonic flight is the SCRAMJET engine, which was studied by the NASA X-43 program. A Supersonic Combustion RAMJET, uses ram compression but maintains supersonic flow through the combustor. Figure 1 below shows the basic setup for a scramjet engine.
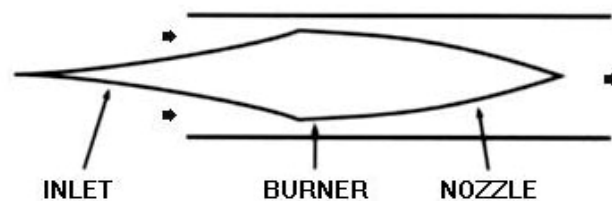
Figure 1. Basic scramjet engine schematic. Arrows indicate flow path direction.

A ramjet uses the speed of the vehicle to compress air coming through the inlet to combustion pressures, and does not use a compressor spool. With few moving parts, scramjets and ramjets are very simple designs.

Current Issues:

The difficulty in achieving success with scramjets is due to the supersonic flow throughout the engine. Numerous problems present themselves during supersonic combustion. Since the inception of the jet engine, the combustion process had taken place under subsonic flow conditions. Supersonic combustion is a more difficult problem. Total pressure losses resulting from shock formation and the short residence time of the flow are two major problems with supersonic combustion. Since the flow is supersonic, any obstruction in the flow path will create shockwaves, resulting in drag losses. With the high speed of the flow through the combustor, the available time to mix fuel into the flow, or spread energy into the flow is short. The short residence time means that the combustor must be lengthened to allow sufficient time to ensure a satisfactory degree of combustion. A longer engine is a heavier engine, and weight is a critical issue in aerospace design.

One method currently used to circumvent this problem is to use a fuel with a very low ignition delay time. The ignition delay time is the time delay from when a given mixture is exposed to a given environment to when that mixture completes the combustion chemical reaction. Hydrogen ignites very quickly and is not as affected by the low residence time as are heavier hydrocarbon based fuels. As will be discussed in Chapter II, the use of hydrocarbon fuels is very attractive due to the reduced amounts of time, effort, and money associated with their use. However, the problem remains as to how to make scramjets operable using hydrocarbon fuels.

Research Focus:

One of the major difficulties with the operability of hydrocarbon based scramjet engines is the ability to spread stable combustion energy into the main flow without disturbing the flow to an extent where unacceptable drag penalties are incurred. Cavity-based flameholders show considerable promise in addressing this problem. Cavity-based flameholders create a subsonic recirculation area of hot combustion products. The subsonic recirculation zone increases the effective residence time for the fuel to ignite, and acts as a pilot light to spread hot combustion products into the main flow.

The performance of cavity-based flameholders can be improved by injecting air along with fuel into the cavity, as shown by Allen (2005). The addition of injected air can aid in optimizing the fuel air mixture within the cavity to allow for the use of the full cavity volume. Increasing the combustion throughout the cavity will result in increased thermal energy spread into the free stream flow. Either as a direct effect, or as an indirect result of increased combustion in the cavity, air injection will most likely lead to increases in total pressure losses. The focus of this research will be to quantify the ability of the air injection technique to spread the combustion energy and products into the main flow and to measure the total pressure losses incurred during the process. Previous investigations have used non-intrusive flow visualization techniques to qualitatively observe the effects of air injection on the cavity's performance. This research uses intrusive probing to gather data on total pressure, total temperature, cone-static pressure, and mixture composition. From these measurements it is possible to quantify the performance of the cavity with different fuel-air injection combinations. This research,

combined with the flow visualization work done previously by Allen (2005), will help determine the true performance advantages or disadvantages of the direct air injection technique over fuel only injection.

Methodology:

Intrusive probing methods were used to sample data in an area of interest behind the cavity ramp. Measurements of static and total pressure, total temperature, and gas mixture were made. This was done over a range of fuel-air injection combinations. The measurement data were used to calculate various aerothermodynamic properties of the flow through the combustor. Temperature measurements of the cavity ramp material were taken in order to analyze the effect of direct air injection on ramp heating.

II. Literature Review

Overview:

The needs and desires of multiple organizations, as well as the general public, bring forward the need for high-speed air-breathing flight vehicles. Airline-like access to space to reduce launch costs or start a fledgling space tourism industry, and national defense purposes such as high-speed aircraft or missiles, have grown the demand for scramjet technology to be taken out of the lab and brought into practical application. Conventional turbojet-based engines typically maximize their specific impulse in the high subsonic regime, with it rapidly decreasing above Mach 1-2. Ramjet engines extend the operable Mach range further into the supersonic regime, and have been in practical use for decades, but they too suffer from decreasing specific impulse in the hypersonic flight regime of interest. Maurice et al. (2000) showed that while ramjet engines begin to suffer a noticeable drop in efficiency above the Mach 3-4 range, scramjets show the ability to extend efficient operation out to the higher flight Mach numbers currently of interest today. Figure 2 below is taken from Weber and MacKay (1958), and it illustrates the basic differences between ramjets and scramjets.

(a) Supersonic-combustion ramjet.

(b) Conventional ramjet.
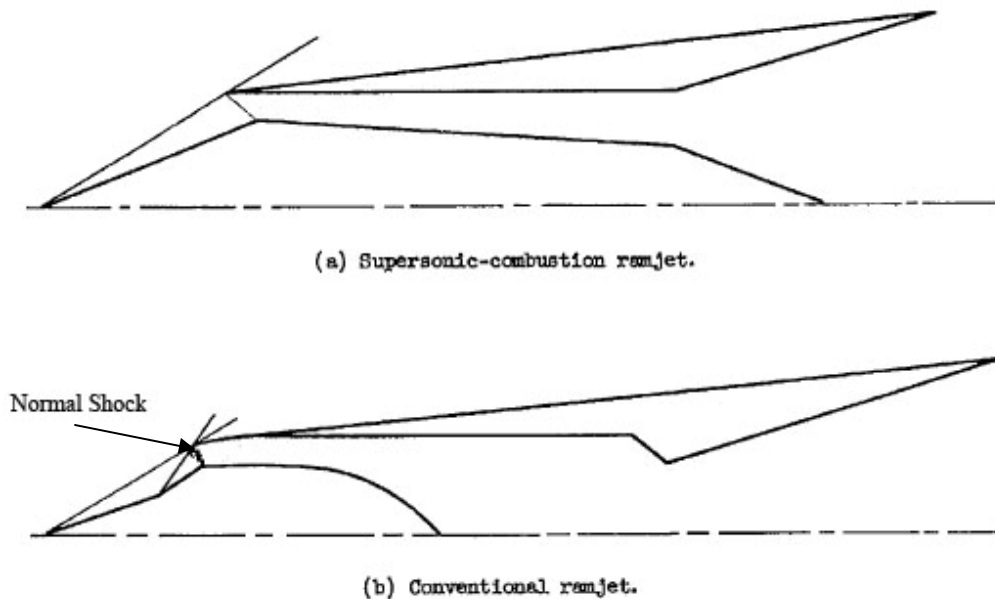
Figure 2. Basic schematic of a scramjet (a) and ramjet (b) engine (Weber and MacKay, 1958; used without permission).

In both diagrams, the outside flow would be supersonic. The most notable differences

between the two designs is the lack of a diffuser section in the scramjet engine, and the

presence of a strong normal shock in the ramjet inlet. This is obviously because the flow

through a scramjet engine is not decelerated below supersonic velocities, and in a ramjet

it is.

The Case for Supersonic Combustion:

The cause of the reduced specific impulse plaguing conventional turbojets and

ramjets at high Mach flight is the need to decelerate the supersonic flow below Mach one.

This typically incurs significant losses in the form of total pressure recovery, even with

advanced inlet design techniques used today. Kutschenreuter (2000) showed the

decreasing total pressure recovery of typical ramjet inlets for higher free stream Mach

numbers. Kutschenreuter showed total pressure recovery less than 50% for Mach numbers greater than 5. The one-dimensional adiabatic energy equations for a perfect gas below (equations 1 and 2) reveal that the decelerating free stream flow from higher Mach numbers results in increasing static temperatures.

$$h_1 + \frac{u_1^2}{2} = h_2 + \frac{u_2^2}{2} \tag{1}$$

$$c_p T_1 + \frac{u_1^2}{2} = c_p T_2 + \frac{u_2^2}{2} \tag{2}$$

As a result, not only does a subsonic combustion engine experience large losses with increasing flight Mach number, but it also experiences increasingly hostile combustor entrance temperatures. Kutschenreuter (2000) also showed the increasing physical demands of high Mach number flight while implementing a subsonic combustion engine. He showed the structural pressure loads and wall heat flux increasing rapidly with higher flight Mach numbers. The high temperatures and pressures the combustor would be required to withstand precipitates the need for extremely durable combustor materials, which are either beyond today's technological capacity or prohibitively heavy or expensive.

Along with the practical concerns of constructing such a device are some thermodynamic ones as well. The high flow temperatures can lead to molecular dissociation. Weber and MacKay (1958) indicated that dissociation can cause non-equilibrium flow losses through improper nozzle expansion. A result of the dissociating oxygen and nitrogen molecules in the air is the presence of their monatomic counterparts. Dooling and Finkenor (1999) discussed the damaging effects monatomic oxygen and

nitrogen can have on the surfaces of some materials. They also indicated that the monatomic species can lead to the formation of nitrous oxides (NO_x). While in the research stage, combustor emissions are not of primary concern. What is of more immediate concern regarding NO_x formations is that oxygen going towards forming NO_x compounds cannot contribute to the exothermic H_2O (as well as CO_2 for hydrocarbon fuels) forming reactions later in the combustion process.

For the reasons discussed above, it is clear then that the practice of subsonic combustion is unsuitable for hypersonic flight. Subsonic combustion, while well understood at today's technological level, is simply too prohibitive to practically, effectively and efficiently achieve hypersonic flight.

Problems Inherent to Supersonic Combustion:

One of the primary advantages to scramjet technology lies in the fact that the flow throughout the combustor is supersonic. The use of a supersonic combustor avoids many of the issues mentioned earlier. However, the supersonic flow through the engine is also the biggest difficulty in developing a practical scramjet engine.

The problem with achieving effective, efficient, stable combustion in scramjet combustors is akin to that of lighting a match in a tornado. The increased speed of the core flow means there is substantially less residence time for the flow to undergo the combustion process. Dixon et al. (2005) and Maurice et al. (2000) showed the residence time of the flow in a scramjet engine is on the order of 0.1-1ms. Maurice et al. (2000) also showed that the physical timescale is shorter than almost all of the intermediate chemical timescales involved in hydrocarbon combustion in Figure 3 below.
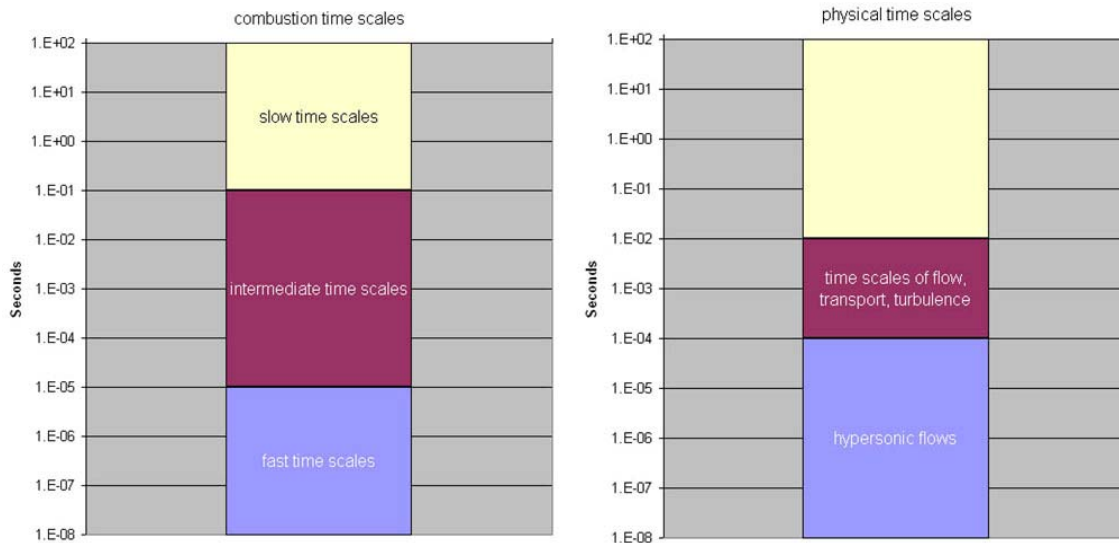
Figure 3. Range of physical and chemical timescales for hydrocarbon combustion
(reproduced without permission from Maurice et al., 2000).

As can be seen, the timescales involved with hypersonic flow are smaller than all but the

fastest of chemical reactions. The disparity between physical and chemical residence

times raise the need for longer, and thus heavier, combustor sections to allow enough

time for efficient mixing and combustion of fuel.

Another problem that is common to supersonic flow is that of shockwaves. At

supersonic velocities any flow path obstruction, whether it is a physical geometric

obstruction or a fuel jet, will create some sort of shockwave from its interference. The

strength of the shockwave can vary as widely as the source can, but each shockwave does

bring with it shock losses.

Finally, the extreme temperatures encountered by scramjets engines are a

byproduct of the high-speed flow in which they operate. In turbojet engines, cool air bled

off of the core flow before combustion is used to cool vulnerable engine parts. With

hypersonic flight there is no low-temperature bleed air that can serve as a coolant.

Thermal management is a significant developmental issue for scramjets. Using the fuel

as a coolant is discussed in Appendix A.

Fuel Choice:

Several ideas have been introduced over the course of scramjet research that are

aimed at increasing the mixing and combustion efficiency without the need for

lengthening the combustor section. Foremost among these ideas is the use of exotic fuels

such as hydrogen.

The use of hydrogen has the benefit of a low molecular weight, which allows for

an engine with a much higher specific impulse, almost three-fold depending on flight

conditions, than one fueled with hydrocarbon fuels such as ethane or ethylene. Paull and

Stalker (2000) demonstrated the higher specific impulse of burning hydrogen as a fuel

rather than ethane or ethylene fuel.

Hydrogen has the added benefit of a shorter combustion time. Since the hydrogen

kinetic reaction chain is a part of any hydrocarbon kinetic reaction chain, its ignition time

is shorter than that of a hydrocarbon by chemical necessity. As shown by Colket and

Spadaccini (2001) and Kutschenreuter (2000), hydrogen has an ignition time on the order

of 10-100 µs. In fact, Kutschenreuter (2000) states that hydrogen-air reactions are not

limited by their chemical reaction rates, but rather by the physical limitations of proper

mixing. In comparison, Colket and Spadaccini (2001) showed that the ignition delay

times for hydrocarbon based fuels, such as ethylene and heptane, are closer to being on

the order of 100-1000 µs. With ignition delay times roughly on the same order of

magnitude as the flow residence time in the combustor, it is difficult for hydrocarbon fuels to progress through the combustion process in the time allotted by the free stream flow. Clearly typical combustion will be too slow for all but the slowest of hypersonic flight velocities. Unless a way can be found to decrease the ignition delay time of hydrocarbon fuels, they will be carried downstream out of the combustor before they have enough time to ignite and impart any energy into the main flow.

The difficulties involved in the use of hydrocarbon fueled scramjet make the fuel choice seemingly obvious. Hydrogen is not only a better performer, as discussed above, but the current level of knowledge regarding hydrogen based scramjets allows for near term development of flight ready engines. Indeed, the NASA X-43A successfully flew last year to nearly Mach 10, breaking the previous atmospheric flight speed record of the X-15. Hydrogen has its drawback however. It is a gas at room temperature, and thus must be stored cryogenically or in heavy pressurized tanks. The higher density liquid hydrocarbon fuels can be stored in conventional aircraft fuel tanks. This is important in designing an engine for an operational craft. Hydrogen is also highly reactive and dangerous to work with. Hydrogen embrittlement affects any tools or storage containers exposed to hydrogen, and the high reactivity of hydrogen makes it a fire hazard. The difficulties the Lockheed Corporation encountered during their research into hydrogen fueled aircraft are detailed in Skunkworks, Rich and Janos (1994). Hydrogen based scramjets may be workable in the civilian sector, or in the quasi-civilian NASA sector, where massive stationary infrastructures are part of normal operations. The use of hydrogen fueled vehicles by military organizations deployed to remote locations with little infrastructure and limited skilled manpower may be less practical.

Hydrocarbon fuels such as kerosene have been in widespread use for over a century now. They are also liquid at room temperature and are not as reactive as hydrogen. This makes their handling easy, and hydrocarbon fuel is used everyday in numerous applications in every kind of operating environment yet encountered. As a final argument for the use of hydrocarbon fuels, they tend to be much cheaper than hydrogen. Maurice et al. (2000) indicated that hydrocarbon fuels are typically an order of magnitude less expensive than hydrogen. The fact remains that for scramjets to run effectively on hydrocarbon fuels, a solution must be found that reduces the time necessary for combustion.

There are a wide variety of different techniques for improving the combustibility of scramjet fuels. They range from different fuel delivery and mixing techniques to modifications of combustor conditions. As they are relevant to the overall discussion regarding the feasibility of hydrocarbon-fueled scramjets, but not of direct relevance to this research, some of these methods are discussed in Appendix A. The method of improving the performance of hydrocarbon-fueled scramjets of direct interest to this research is cavity-based flameholding.

Cavity Flameholders:

Cavity flameholders create a subsonic region for a recirculating trapped vortex to exist. Fuel and air can be entrained from the free stream flow into the cavity through the shear layer, or directly injected into the cavity itself. The trapped vortex concept has been shown by Ben-Yakar and Hanson (1998) to be an excellent method of

providing a stable flameholding device. However, it is this same stability which limits

the amount of turbulent mass entrainment with the free stream flow.

Cavities are normally classified as open or closed. An open cavity is one in which

the shear layer separates at the cavity leading edge and reattaches on the aft edge. A

closed cavity is one in which the shear layer is unable to reattach to the aft end of the

cavity, and thus attaches to the cavity floor instead. Figure 4 illustrates the geometric

classification of cavities. Nestler et al. (1968) determined that the length to depth ratio

separating open and closed cavities was approximately 10.

a) Open cavity flow ($L/D < 10$)

b) Closed cavity flow ($L/D > 10$)
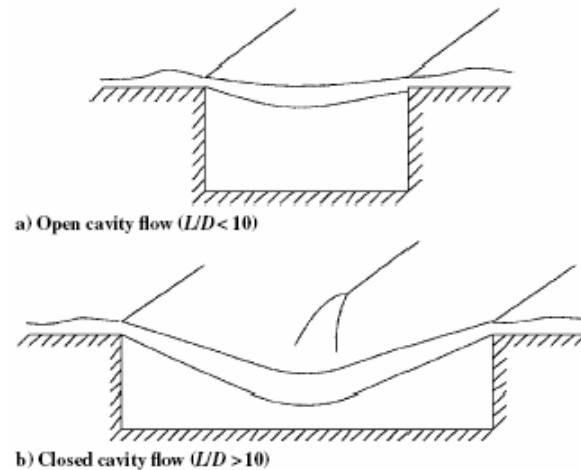
Figure 4. Two general classifications of cavities a) open cavity and b) closed cavity
(Gruber et al., 2001; used without permission).

Ben-Yakar and Hanson (1998) determined that cavity length most directly affects mass

entrainment between the cavity and free stream, and cavity depth most affects the cavity

residence time. They also summarized that cavities with higher L/D values produced

more drag. Typically the fuel of choice determines the required residence time, and thus

establishes the required cavity depth. In order to increase mass entrainment, the amount

of fuel-air mixture drawn into the subsonic recirculation region in the cavity, the cavity length must be increased. It is important to maximize the mass entrainment since the goal of the cavity flameholder is to provide a stable region in which subsonic combustion can occur away from the free stream flow. Although lengthening the cavity increases mass entrainment, increasing the cavity length will also result in increased drag, as stated by Ben-Yakar and Hanson (1998).

While the leading edge of a cavity is almost always at an angle 90° to the free stream, the aft edge angle can be varied greatly. In addition to varying the angle of the aft cavity wall, its height above the cavity floor can also be varied. The ratio of leading edge cavity wall height to aft cavity wall height is known as the offset ratio. Gruber et al. (2001) found that increasing the offset ratio greater than one leads to significant form drag from pressure losses resulting from the strong expansion wave separating on the leading edge. An example of the aforementioned phenomenon is shown below in Figure 5.
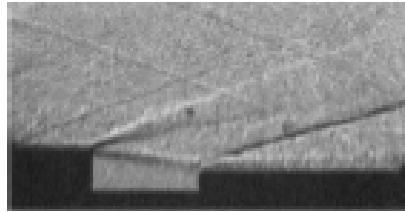
Figure 5. Strong expansion fan off of cavity leading edge for offset ratio greater than unity (Gruber et al., 2001; used without permission).

Gruber et al. (2001) showed that decreasing the aft cavity wall angle from 90° (perpendicular to cross flow) and lengthening the cavity for a pre-determined depth resulted in greater pressure losses. The increased losses, in both cases, are caused by the shear layer extending down the cavity's angled aft ramp, which exposes more area of the

15

aft ramp to high pressure. Gruber et al. (2001) theorized that the shear layer extending

down the cavity ramp would increase mass entrainment. They also showed that

decreasing the aft wall angle resulted in increased stability of the cavity flow. Thus there

is a tradeoff between stability and drag. The general setup of the cavity studied in this

research was the same as that studied by Gruber et al. (2004) and Allen (2005), an open

cavity with a L/D ratio of 4 and a 22.5° aft ramp angle.

Two recirculation vortices are formed within the cavity, an unburned fuel-

rich vortex near the cavity step and a primary vortex undergoing mass exchange with the

free stream flow. Figure 6 shows a CFD calculation by Gruber et al. (2001) of the typical

fuel-air distribution within a cavity (darker shades correspond to fuel rich regions).
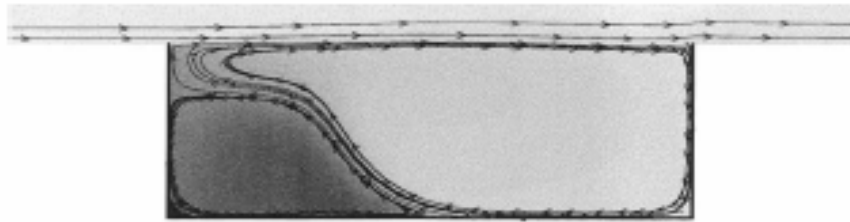
Figure 6. Fuel distribution in a closed cavity flameholder. Darker shades indicate
fuel-rich regions (Gruber et al., 2001; used without permission).

Gruber et al. (2004) concluded that the presence of the fuel-rich lobes limited the

combustion in the upstream portions of the cavity and caused fluctuations in the

downstream cavity burning. It seems then that the cavity's double vortex structure limits

the effectiveness of increasing fuel input as a means of increasing combustion within the

cavity. Ben-Yakar and Hanson (1998) suggested that the mass entrainment can be

improved with the addition of fuel or a fuel-air combination within or upstream of the

cavity. Gruber et al. (2004) showed direct injection of fuel into the cavity flameholder to

be an improvement over other forms of fuel injection such as upstream injection. They noted a more uniform fuel-air mixture within the cavity, and increased robustness and stability of the cavity's flameholding ability.

Allen (2005) investigated the effects of adding air injection with fuel injection directly into the cavity as a means of improving the fuel-air mixture within the cavity. He followed on the work of Gruber et al. (2004) at the Air Force Research Lab at Wright-Patterson AFB using their same cavity. Allen (2005) showed that the use of air injection was successful in improving the combustion in the cavity, particularly near the forward cavity step where the fuel-rich secondary vortex is located. It seems clear that the additional air directly injected into the cavity improved the fuel air mixture, especially near the forward step, to a point that allowed for increased combustion. It should be noted that Allen (2005) also observed that the air injection technique did not have merely a linear effect on the fuel-rich region. Increasing the air injection without bound had diminishing effect, and eventually a reverse effect. For lower fuel injection rates, if the air injection was increased to its maximal limit the combustion increases seen at lower air injection rates diminished to levels near the original fuel-only case. It would seem that the direct air injection technique is able to cause the cavity fuel-air mixture to become too lean to gain any improvements in combustion if the air injection rate is not controlled.

Allen (2005) also showed that increasing the amount of cavity combustion effectively raised the flame shear layer, causing it to reattach further up the aft ramp. He theorized that this would lead to reduced drag on the cavity.

Summary:

Supersonic combustion of heavy hydrocarbon fuels remains a difficult problem. Much research over the past decade has worked towards improving mixing technologies and reducing the ignition time of hydrocarbon fuels. Hydrocarbon fuels are an attractive fuel source due to the ease with which they are handled and stored. One method that has proven effective in increasing the mixing of a combustible mixture into the core flow is the use of cavity flameholders. Cavity flameholders have been shown to be robust flameholding devices that do not cause as much of drag penalty as other passive mixing devices such as strut injectors. Cavity flameholders employing direct fuel injection do suffer from the presence of a non-combusting fuel-rich area near the bottom of the forward cavity step in that this is essentially wasted cavity volume. The added injection of air into the cavity serves as a means to tune the fuel-air mixture within the cavity to promote combustion throughout a greater portion of the cavity. It also effectively extends the upper fueling limit that will achieve a combustible cavity mixture. Without direct air injection, the unbounded addition of fuel offers little improvement in combustion due to an increasing amount of cavity volume becoming too fuel-rich. Adding air injection allows for a larger fuel mass to be injected into a given cavity volume while still yielding effective combustion.

Research Focus:

This research focused on obtaining measurements of static pressure, total temperature, and total pressure as a means of determining the quantitative performance of the cavity for different fuel-air injection ratios. Combining the data gained from

quantitative measuring with flow-visualization data already obtained provided insight as to what physical benefits and costs are associated with the use of direct fuel and air injection into cavity flameholder in a supersonic flow. This research determined what changes in enthalpy spread to the free stream flow were associated with the increased combustion indicated qualitatively by Allen (2005) for a given fuel-air setting. Total pressure losses were also measured, and showed how the visually observed increases in combustion translated into quantifiable flow losses. In addition, gas mixture data were gathered in order to examine what changes in flow mixture occur at the cavity exit for a given fuel-air mixture. Ramp heating temperatures were investigated to see how a certain fueling scheme affected the material temperature experienced by cavity.

III. Methodology

Test Facility:

The test facility used is located in the Air Force Research Lab Propulsion Directorate complex in test cell 19. Its design and construction is discussed by Gruber and Nejad (1994). The Research Air Facility is capable of supplying a continuous flow of 30 lbm/s of air heated up to 1000 ºF and pressurized up to 500 psia. Figure 7 is a schematic of the facility input system and the test section.
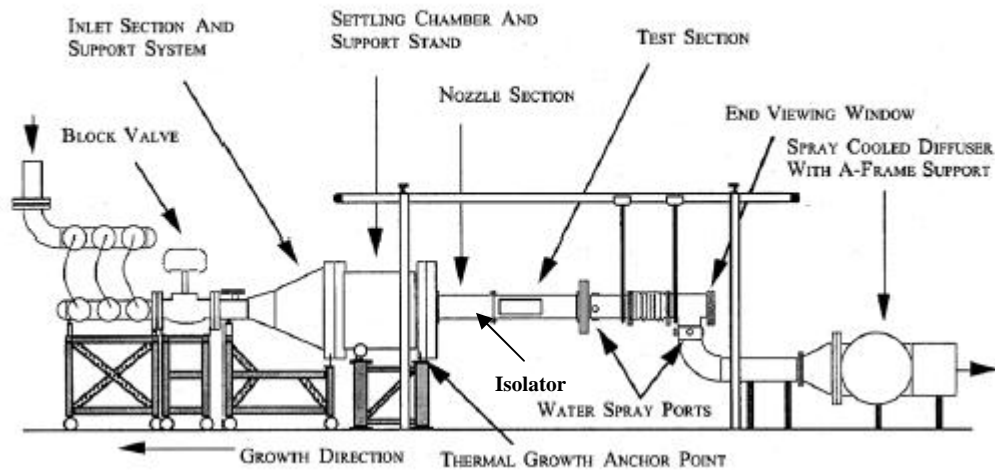
Figure 7. Schematic of wind tunnel facility (Gruber and Nejad, 1994; used without permission).

The air flows into the settling chamber and into the test section isolator through a Mach 2 convergent-divergent nozzle. The isolator is 7 in long, 6 in wide, and 2 in high, and functions to prevent the increased pressure due to combustion from interfering with the nozzle. Proceeding downstream from the isolator is a diverging ramp of length 29 in and angle 2.5º.

Test Section:

The free stream conditions supplied to the test section were Mach 2 flow with total pressure of 80 psia and total temperature of 580 °F. The free stream total pressure and temperature were measured in the settling chamber and supplied to the tunnel control computer for adjustment. These free stream conditions were selected to match those studied by Allen (2005). The conditions simulate Mach 4 flight conditions. A cut-away picture of the test section used in this research can be seen in Figure 8 below.
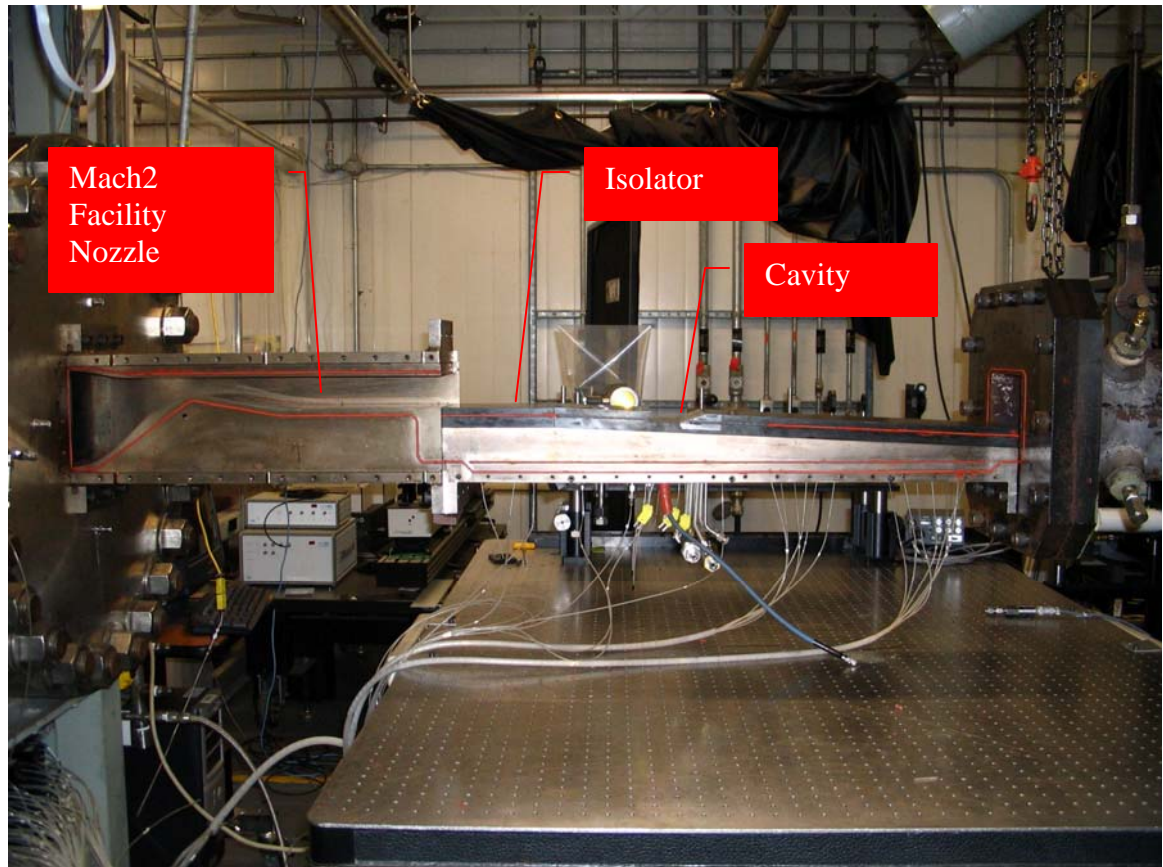
Figure 8. Wind tunnel test section with top and sidewalls removed.

The cavity flameholder investigated during this research is of the same design discussed by Allen (2005). The recessed cavity is mounted with the top edge flush with

the diverging ramp section, and is 2.6 in long by 6 in wide by 0.65 in deep, The recessed

cavity has a forward step at a 90° degree angle and a 22.5° degree aft ramp angle.   The

cavity is shown in Figure 9.
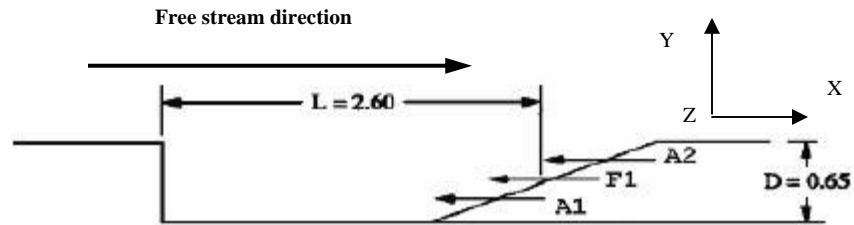
Figure 9. Cavity flameholder diagram with free stream flow left to right. A1 and
A2 show air injection ports, and F1 shows the fuel injection port.

Fueling:

Located on the ramp are three rows of injector ports aligned parallel to the cavity

floor (the injection direction matches the arrows for A1, A2, F1 in Figure 9), with the top

and bottom rows for injecting air and the middle row for injecting fuel. Figure 10

displays the fuel and air injector setup.
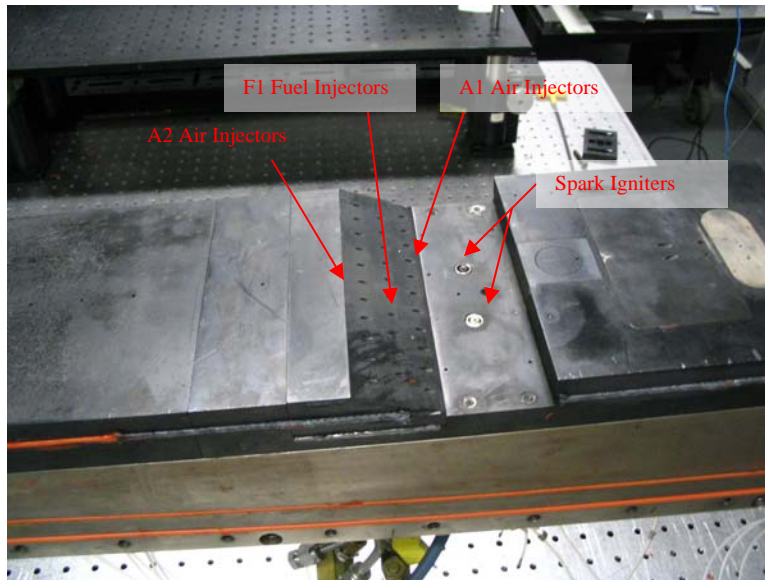
Figure 10. Fuel and air injection setup within the cavity.

There are 10 fuel injector ports of 0.063 in diameter, and two rows of 11 air injector ports of 0.078 in diameter. They are at locations F1, A1 and A2 respectively in Figure 9. Only the lower air injection row, location A1 in Figure 9, was used in order to compare with Allen (2005). Fuel was delivered from high pressure storage bottles, and regulated via a dome pressure regulator that was actuated by a PC in the control room. Fuel and air were injected at 10.5 psia and 7.5 psia respectively, and were controlled by a pair of Tylan General mass flow controllers. Fuel and air flow rates were set manually for each run with a Tylan General flow meter. The Tylan controllers are factory calibrated with air being the output. Thus if another gas is used, a correction factor must be used. Since ethylene was used as the fuel, a correction factor of 0.6, as stipulated in the Tylan users manual, was used. The maximum flow rate of the air controller was 500 SLPM, and the maximum flow rate for the fuel controller was 200 SLPM. Thus, after applying the correction factor, a 100% flow rate would correspond to 500 SLPM of air, and 120 SLPM of ethylene. Seven fuel-air combinations were tested. These combinations were chosen to match test conditions of previous research. These combinations, as well as their corresponding flow rates and equivalence ratios, are displayed in Table 1 below.

Table 1. Fuel-air test combinations.

Fuel %	Air %	Fuel Flow (SLPM)	Fuel Flow (g/s)	Air Flow (SLPM)	Air Flow (g/s)	Cavity Equivalence Ratio
0	0	0	0	0	0	N/A
32	0	38.4	0	0	0	∞
32	30	38.4	0.73	150	2.95	0.77
32	70	38.4	0.73	350	6.88	0.33
50	0	60	0.73	0	0	∞
50	50	60	1.14	250	4.91	0.72
50	100	60	1.14	500	9.82	0.36

The equivalence ratios displayed above are calculated by relating the ratio of fuel and air injected to the stoichiometric combustion equation below.

$$1C_2H_4 + 3(O_2 + 3.76N_2) \rightarrow 2CO_2 + 2H_2O + 11.28N_2 \tag{1}$$
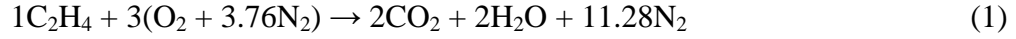
The stoichiometric fuel to air ratio is found from equations 2 and 3 below.

$$(Fuel/Air)_{Stoich.,mass} = (1/3)*(MW_{fuel}/MW_{air}) \tag{2}$$

$$(Fuel/Air)_{Stoich.,mass} = 0.068 \tag{3}$$

The equivalence ratio of the cavity injectants can be found from equations 4, 5, and 6.

$$(Fuel/Air)_{Actual} = (SLPM_{fuel}/SLPM_{air})*(MW_{fuel}/MW_{air}) \tag{4}$$

$$\varphi = (Fuel/Air)_{Stoich.} / (Fuel/Air)_{Actual} \tag{5}$$

$$\varphi = 3*(SLPM_{fuel}/SLPM_{air}) \tag{6}$$

Note that the equivalence ratios displayed in Table 1 are only for the fuel and air injected into the cavity, and do not account for free stream air entrainment into the cavity. For all fuel-air combinations, spark plugs were used to initiate combustion, but were turned off after combustion was established. Fuel valves, air valves, and spark plugs were all operated via a PC in the control room.

Probe Setup:

For this research, probing was done along 2 axes, vertical (Y-axis) and spanwise (Z-axis). A vertically moving sidewall allows the probe to be traversed along the Y-axis. The moveable sidewall is sealed against the stationary sidewall with an O-ring style seal. During this research the sidewall was fixed in the streamwise direction. The streamwise positioning of the probe tip is discussed later. Cut through this sidewall is a diamond shaped hole 0.875 in wide by 0.25 in tall, through which the probe strut can be inserted. Figure 11 shows a probe inserted into the sidewall in the configuration previously described.

Figure 11. Moveable sidewall with diamond-shaped probe strut hole.

This allows for the probe to be traversed along the Z-axis. The probe can be traversed real-time along both Y and Z axes, but in order to limit the stress on the O-ring sealer, the probe is fixed at a Y-axis coordinate, and traversed along the entire Z-axis for each run condition before moving to the next Y-axis position. The traversing mechanism was built in-house at AFRL/PRAS using Parker Compumotor encoders, and is operationally

accurate to 0.001 in along both the Y and Z axes. The traversing mechanism can be seen in Figure 12.
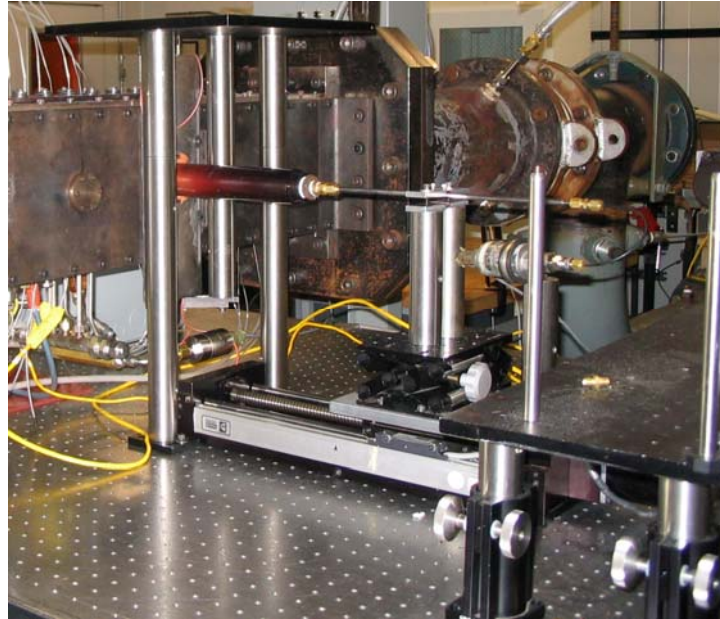
Figure 12. Traversing mechanism and movable tunnel sidewall.

For the pitot and cone static pressure measurements and the total temperature measurement, data were taken along the Y-axis from 0.125 in off the divergent ramp floor to 0.5 in off the ramp floor in increments of 0.125 in. Data were also taken at a Y-axis height of 1.0 in to estimate the validity of set free stream conditions. At each elevation, data were collected along the Z-axis from 0 in off of the sidewall to beyond the test section centerline (3 in from sidewall) at 3.5 in off the sidewall in 0.125 in increments. The probes were traversed in the Z-axis direction automatically by a computer during a test run. The settling time for each data point was 0.25 seconds. Figure 13 below shows the placement of the data points within the test section.
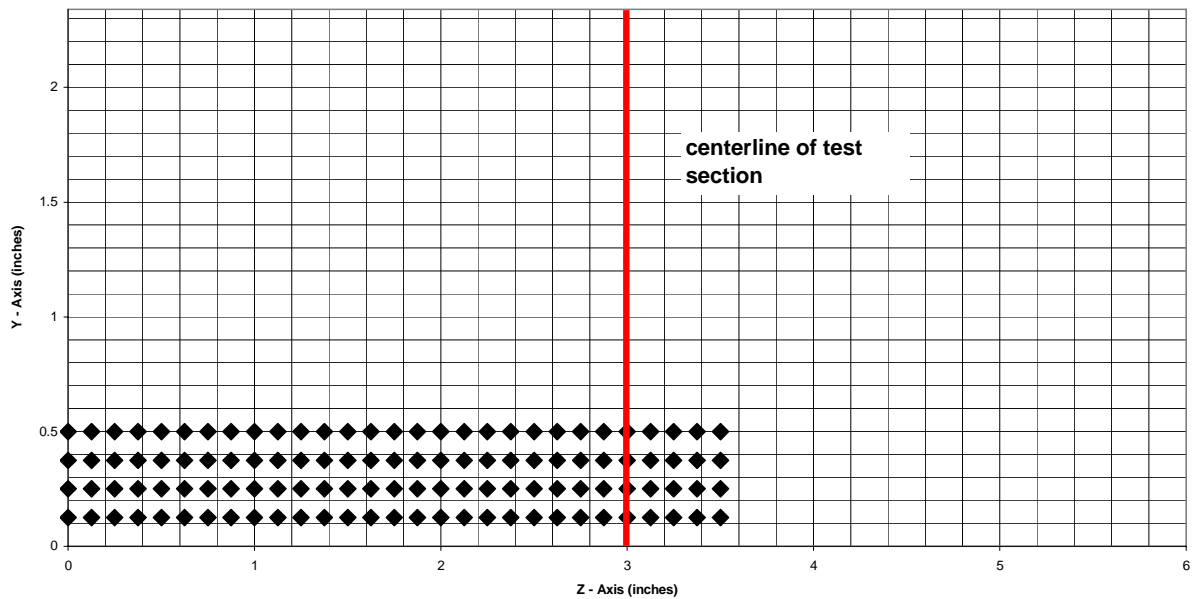
Figure 13. Data point grid in relation to test section geometry. Cavity would extend below Z-axis. Flow is out of page.

Note that the zero value of the Y-axis corresponds to the divergent ramp floor, and thus the cavity, located upstream (into the page), would extend below the Z-axis. The lowest Y-axis value was 0.125 in due to the geometry of the probe. The probe diamond was 0.25 in tall, and the upstream-facing probe tube was 0.125 in in diameter. The probe tube centerline was offset from the diamond centerline by 0.0625 in. An additional 0.0625 in was allowed between the bottom of the diamond and the ramp floor to prevent binding on the probe strut after thermal expansion takes place. Thus the lowest attainable Y-axis value was 0.125 in off the ramp floor. This is illustrated in Figure 14.
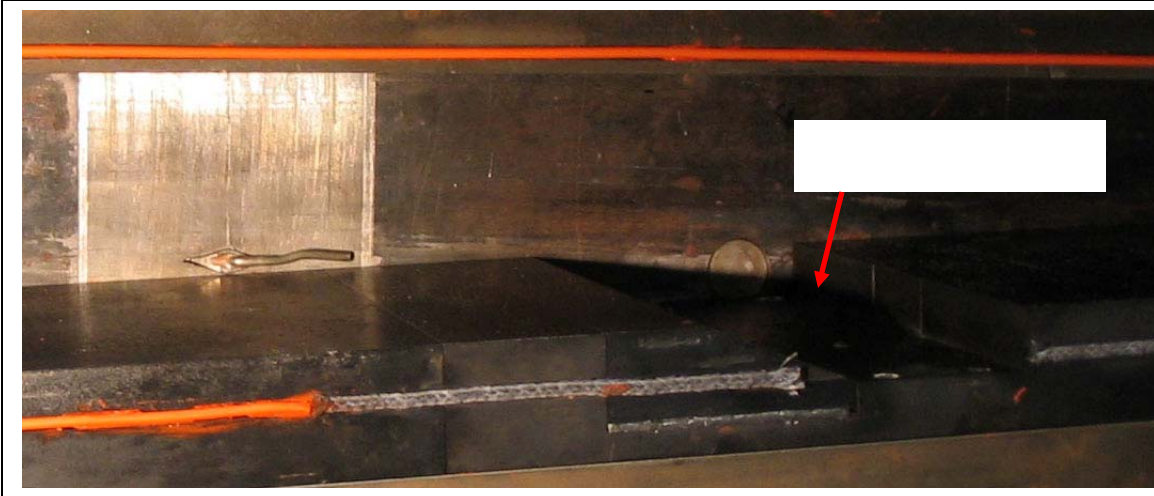
Figure 14. The offset of the pitot pressure tube and the diamond shaped supporting strut limited the minimum Y-axis probe location.

The highest Y-axis position where data was taken was found by starting the probe at 1 in off the ramp floor, and proceeding downward towards the ramp floor until significant measurement gradients were observed. This allowed for the greatest possible resolution within the area of interest. The upstream-facing probe tube was 1.5 in long. All probing was done with the probe tip at a streamwise location approximately 2.25 in behind the aft edge of the cavity ramp (approximately 5.6 in behind the forward cavity step). This location was a compromise between the desire to collect data as near the cavity as possible and the practical concern of probe integrity so close to the high temperature cavity environment. For this research data were only taken up to slightly past the spanwise centerline. Gruber and Nejad (1994) demonstrated the flow through the AFRL Test Cell 19 wind tunnel was symmetrical. Data beyond centerline were used to verify tunnel symmetry. No measurements beyond spanwise centerline were taken for the gas sampling measurements, which will be discussed in further detail later in this chapter.

Pitot Pressure:

The Pitot pressure probe was a straight tube mounted on the end of a diamond shaped strut. The tube had a blunt open-ended nose, and was approximately 1.5 in in length, with an outer diameter of 0.125 in and an inner diameter of 0.0625 in. Figure 15 displays the pitot probe used.
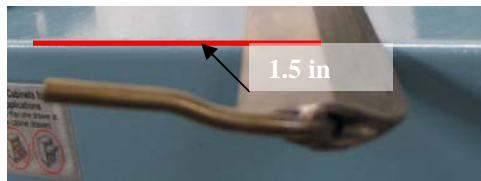
Figure 15. Pitot pressure probe.

Open-ended pitot probes such as the one just described are very resistant to inaccuracies induced from being misaligned with the flow. Liepmann and Roshko (1985) showed pitot pressure probes can maintain 1% accuracy while being misaligned up to 20°. The tube fed through the strut and into a Honeywell absolute pressure transducer of 0.25% full-scale psi accuracy. The transducer was calibrated to 100 psia full-scale before each set of test runs using a Druck secondary calibration standard. The pressure transducer fed into a National Instruments SB series input module of 0.2% full-scale psi accuracy. The input module fed into a National Instruments 16-bit analog-to-digital data acquisition board, which interfaced with a PC. All data were stored on the PC.

Cone Static Pressure:

A cone of 10° half angle on the end of a 1.5 in long 0.125 in diameter tube was used to obtain the cone static pressure. Four concentrically equal spaced static pressure

holes were located approximately halfway along the cone surface in the streamwise direction. These fed into a common tube, which connected to a Honeywell absolute pressure transducer. These 4 holes give a pneumatic average, and help correct for any misalignment that may result from imperfect machining or assembly. The data acquisition follows the same path as with the total pressure. Figure 19 displays the cone static pressure probe.

Figure 16. Cone static pressure probe.

Total Temperature:

The total temperature probe had the same basic geometry of the previous two probes discussed. The ceramic probe tip had two equally spaced aspiration holes, and within the probe tip was a type-k thermocouple of ±1 °F accuracy. The voltage from the thermocouple then fed into the same National Instruments SB series input module of 0.2% full-scale psi accuracy and National Instruments 16-bit analog-to-digital data acquisition board used for the pitot and cone-static pressure measurements. The total temperature probe is displayed below.

Figure 17. Total temperature probe.

Gas Sampling:

To obtain gas species data, an ECOM KL portable emission analyzer was used to obtain mole fractions of O_2, NO, NO_2, CO, and unburned hydrocarbons (C_xH_y). The ECOM KL analyzer is displayed below in Figure 18.
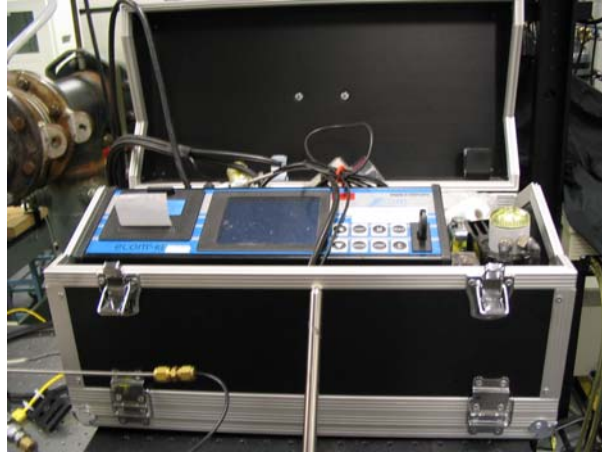
Figure 18. ECOM KL gas analyzer.

Test gas was drawn into a tube of geometry identical to the pitot pressure tube and into the ECOM gas analyzer unit. The gas sampling probe had an internal divergence within the tube so as to allow for the capture of an undisturbed stream tube of flow gas. The internal divergence swallows the normal shock ahead of the probe, which prevent gas spillage around the probe tip. Air taken into the gas analyzer immediately passes through a desiccant, providing dry measurements. The unit interfaced directly with a PC, and all data were stored on the PC. For the data gathering process for the species measurements, no automatic traversing was possible and all points were sampled individually. There is a certain amount of delay time from when the cavity is ignited and the tunnel running to when the ECOM unit can send steady data. Thus to gather species data at a given y-z

coordinate the analyzer must run for up to a minute for the species data to plateau to a

point where point values could be approximated. Certain fuel-air combinations (typically

those with no air injection) caused the cavity ramp to heat up beyond acceptable material

safety limits and thus a full minute of data would not be gathered. The data processing

side of this difficulty will be discussed in Chapter IV. The result of this lengthy data

acquisition process was that the data grid for the species data needed to be coarsened.

Figure 19 shows the data grid for the gas sampling.
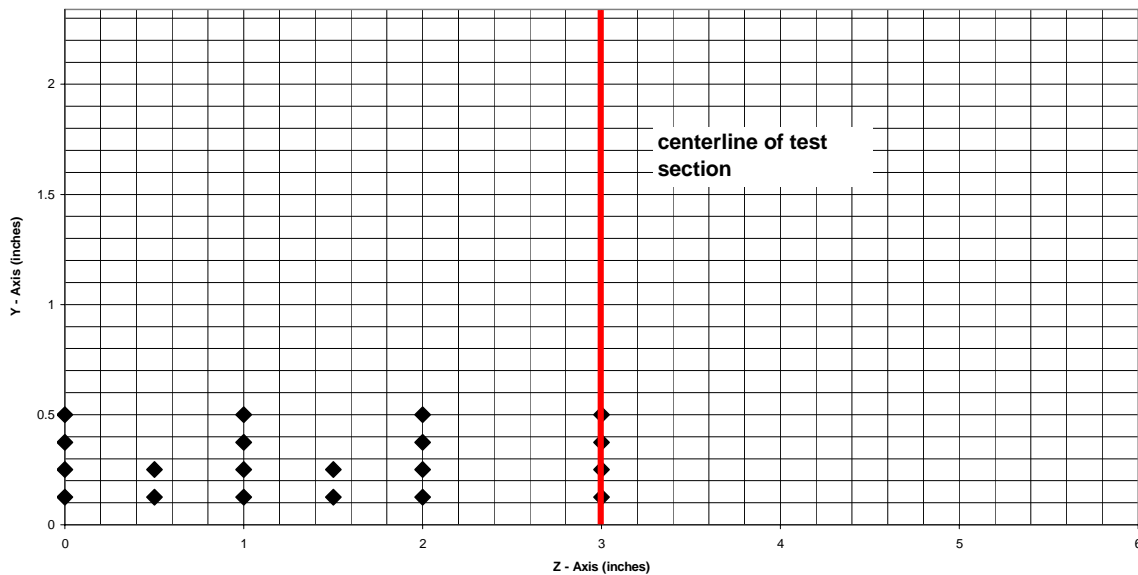
Figure 19. Data point grid for gas sampling procedure relative to tunnel geometry.
Cavity would extend below Z-axis. Flow is out of page.

There are more data points closer to the combustor floor because it was here in which the

greatest change from free stream was observed, and it was necessary to better define the

species distribution. Also, data were only taken up to the spanwise centerline, and not

beyond, in order to obtain as fine a resolution for the area of interest as possible.

Cavity Ramp Heating:

For material safety concerns, a given test run was terminated if the ramp temperature exceeded 1000 °F. This typically gave 40-60 seconds of continuous data sampling at a time. Numerous tunnel operating conditions, including cavity ramp material temperature, were monitored via a National Instruments SCXI 1102 subsystem that interfaced with a PC. The subsystem allowed for recording time plots of ramp temperature for each fuel-air combination. From this data one can discern material heating effects between the various fueling schemes such as peak temperature reached and the amount of time elapsed before a set reference temperature was reached.

Data Processing:

All data were recorded as text or Microsoft Excel-based files. Microsoft Excel was used to manage the data. The total pressure, cone-static pressure, and total temperature were input into a data reduction code, discussed in Fuller et al. (1992), which iterates through the isentropic flow relations, perfect gas relation, Pitot-Rayleigh, and Taylor-Maccoll equations to arrive at solutions for Mach number, total and static pressure and total and static temperature, static density, bulk velocity, specific heat ratio, sound speed, enthalpy, mass flux and momentum flux ahead of the probe shock. The data reduction code is capable of accepting binary gas mixture concentrations, but due to combustion there will be multiple different gas species in the mixture. However, the mass flow rate of the fuel injected was small compared to the core flow rate of air through the combustor. Table 1 shows the maximum fuel injection mass flow rate to be 1.14 g/s. The tunnel free stream conditions of 580 °F, 80 psia and Mach 2 yield a mass

flow rate through the area of interest (0.125 in to 0.5 in along Y-axis, 0 in to 3.5 in along Z-axis) of approximately 400 g/s. Furthermore, as will be shown in Chapter IV, the results from the gas sampling research showed very small changes in gas composition from air, with the maximum change in oxygen concentration being a decrease from 21% oxygen to 19% oxygen. Appendix B shows the variation in specific heat ratio from that of air for the measured gas mixtures to be small. Thus, assuming air only for the data reduction code should allow a good degree of accuracy in determining pertinent data ahead of the probe shock. The data reduction code guesses a temperature (T_1) and calculates the specific heat ratio (γ) from Equation 9 and a look-up table for the constant pressure specific heat.

$$\gamma = \frac{\dfrac{c_p(T_1)}{R_{gas}}}{\dfrac{c_p(T_1)}{R_{gas}} - 1} \tag{9}$$

The Taylor-Maccoll equation is shown in Equation 10, and the Pitot-Rayleigh equation is shown by Equation 11.

$$\frac{P_c}{P_1} = 1 + \frac{\gamma M_1^2}{2} \frac{(P_c - P_1)}{q_1} \tag{10}$$

$$\frac{P_{t,2}}{P_1} = \left(\frac{(\gamma+1)M_1^2}{2} \right)^{\frac{\gamma}{\gamma-1}} \left(\frac{\gamma+1}{2\gamma M_1^2 - (\gamma-1)} \right)^{\frac{1}{\gamma-1}} \tag{11}$$

Dividing Equation 10 by Equation 11 yields Equation 12.

$$M_1 = f(Pc / P_{t,2}, \gamma) \tag{12}$$

The Mach number ahead of the shock can be found from the ratio of static pressure measurement on the cone-probe surface and pitot pressure, along with the specific heat ratio. Equation 12 is solved via a look-up table described in Fuller et al. (1992). The guessed temperature can be checked via the isentropic temperature relation in Equation 13, assuming $T_{t,1} = T_{t,2}$ for adiabatic flow.

$$T_1 = T_{t,2}\left(1 + \frac{\gamma-1}{2}M_1^2\right)^{-1}$$ (13)

The data reduction code iterates on temperature until a solution is reached. With the Mach number known Equation 11 can be solved to give the static pressure ahead of the probe shock (P_1). Using the isentropic pressure relation in Equation 14 the total pressure ahead of the probe shock can be solved for.

$$P_{t,1} = P_1\left(1 + \frac{\gamma-1}{2}M_1^2\right)^{\frac{\gamma}{\gamma-1}}$$ (14)

The density is calculated from the perfect gas relation in Equation 15.

$$\rho_1 = \frac{P_1}{R_{gas}T_1}$$ (15)

Sound speed is found from Equation 16.

$$c_1 = \sqrt{\gamma R_{gas}T_1}$$ (16)

Velocity is determined from the Mach number found through Equation 12 and the relation in Equation 17.

$$u_1 = M_1 c_1$$ (17)

The mass and momentum fluxes can then be found from Equations 15 and 17, as shown in Equations 18 and 19.

$$\frac{\dot{m}_1}{A} = \rho_1 u_1 \qquad (18)$$

$$\frac{\dot{p}_1}{A} = \rho_1 u_1^{\,2} \qquad (19)$$

Enthalpy is found from Equation 20, and total enthalpy is found from equation 21.

$$h_1 = \int_{T_0}^{T_1} Cp(T)dT \qquad (20)$$

$$h_{t1} = h_1 + \frac{u_1^{\,2}}{2} \qquad (21)$$

Since the constant pressure specific heat is a function of temperature, Equations 20 and 21 do not vary linearly with temperature. The data reduction code would store all these values for the entire range of Y and Z coordinates to computer file. Gas mixture data was reported by the ECOM-KL gas analyzer unit in units of parts per million and percentage. All data from the gas analyzer were converted to percentages for comparison. Uncertainty analysis of the reduced data quantities is described in Appendix B.

It should also be mentioned that while each different measurement was taken at a different point in time, Gruber and Nejad (1994) demonstrated the test section in Test Cell 19 has highly repeatable flow, and it was assumed for this research that each separate measurement can be attributed to its Y-Z coordinate regardless of the measurements not occurring simultaneously.

IV. Results and Analysis

Results:

During this research four separate measurements were taken along a plane aft of the cavity flameholder. Cavity combustion was established and maintained for all fuel-air settings with all four measurements. Two problems were encountered during the investigation. During the first night of testing, thermal expansion of the tunnel in an unexpected direction (Y-axis) led to the pitot probe impinging on the tunnel floor and some resultant damage to the probe body. This damage was repaired by the lab technicians and the pitot probe was used at a later testing date. The other problem was alluded to in Chapter III. The length of time necessary for gas mixture values to reach steady state at times exceeded the amount of continuous run time available, as limited by cavity ramp material heating concerns. As a result some of the gas mixture data were not at a steady state condition when sampling was discontinued. Fuel air combinations which posed the greatest problem for shortened run time were 32% Fuel – 0% Air, 32% Fuel – 30% Air, and 50% Fuel – 0% Air. Thus gas mixture data at these fuel-air settings may not be completely representative of the true gas mixture. At higher air injection levels the air helped cool the cavity ramp and allowed full run times. Other than the two problems mentioned previously, all data were successfully gathered and processed.

Analysis:

The measurements of cone static and pitot pressure and total temperature were all representative of values behind the shockwave induced by the probe body. Thus a data reduction technique developed by Fuller et al. (1992), and described in Chapter III was

used to solve through the ideal gas, Taylor-Maccoll and Pitot-Rayleigh equations, and the isentropic flow relations, while iterating the specific heat ratio against temperature.

Baseline Flow:

The baseline (no fuel or air injection) flow was examined to determine the effects of the cavity alone. Figure 20 shows the Mach number distribution for the probed area.

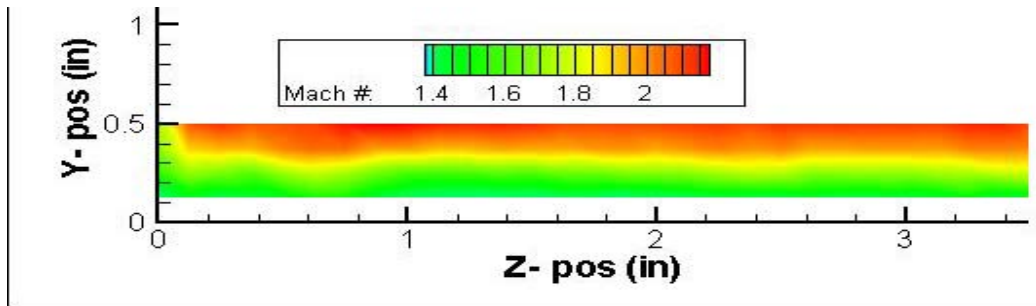Figure 20. Mach number distribution behind cavity ramp for non-reacting flow (flow out of page).

As expected, the Mach number decreases near the tunnel sidewall and floor due to boundary layer effects. No obvious flow phenomena are visible from Figure 20. Figure 21 below shows the static temperature distribution.
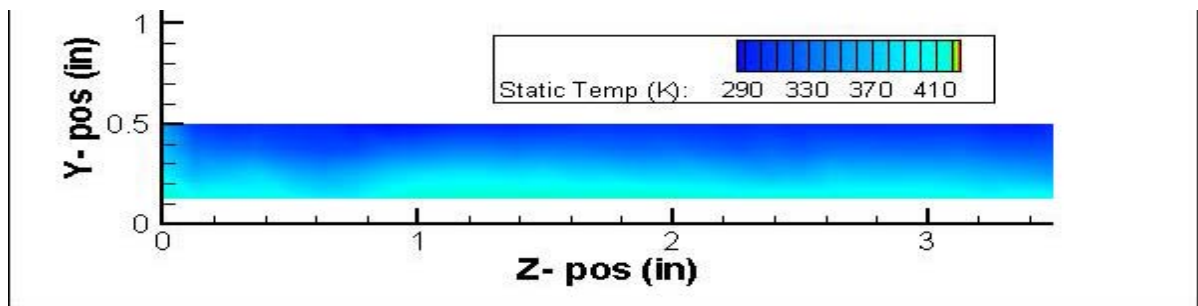

Figure 21. Static temperature distribution behind cavity ramp for non-reacting flow (flow out of page).

As can be seen the temperature near the tunnel floor and sidewall is higher than in the free stream. This is due to the reduced Mach number in these same areas. One thing to note from Figure 21 is the presence of a lobe of higher temperature located from $0.8 < Z < 2.2$ in. The lobe structure is seen often in many of the plots in this chapter, and is most likely the result of the three-dimensional recirculating primary vortices within the cavity. Combustive heat release is greatest in these structures, and their effects are seen in the contour plots of multiple variables. The total temperature distribution below in Figure 22 shows a region of elevated total temperature approximately $0.2 < Y < 0.4$ in above the tunnel floor. The tunnel free stream total temperature was set to 580 °F (578K).

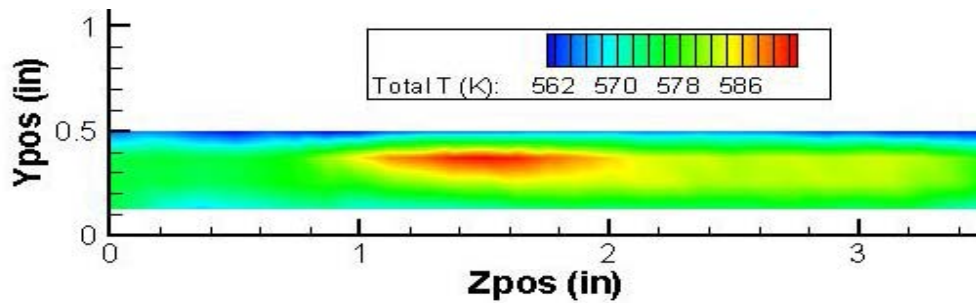Figure 22. Total temperature distribution behind cavity ramp for non-reacting flow (flow out of page).

Both the high total temperature region and the high static temperature lobe share the same Z-axis boundaries.

The lobe structure is present in the total pressure distribution shown below in Figure 23. Tunnel free stream total pressure was set to 80 psia (551600 Pa). Again the phenomenon is located between $0.8 < Z < 2.2$ in.
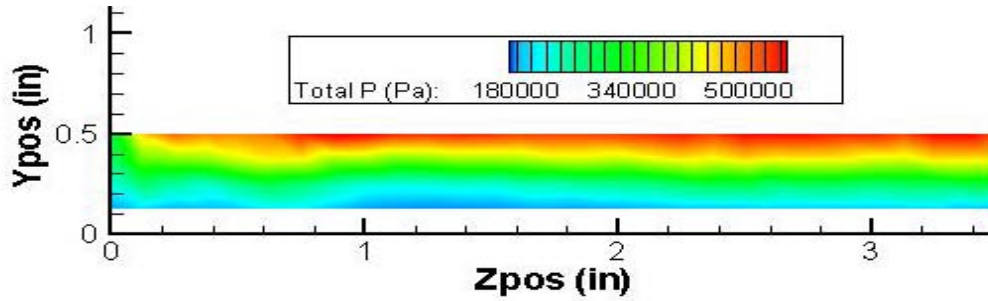
Figure 23. Total pressure distribution behind cavity ramp with flow out of page.

The final interesting phenomenon regarding the baseline cavity flow field can be seen in the static pressure distribution shown below in Figure 24. There is a pair of low pressure regions separated by a high pressure region at the tunnel midspan line.
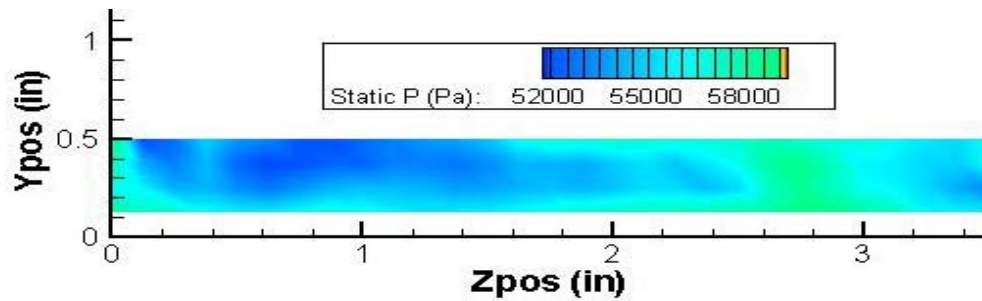
Figure 24. Static pressure distribution behind cavity ramp with flow out of page.

The region of elevated temperature and reduced pressure is most likely a result of the free stream flow interacting with the cavity shear layer and the tunnel sidewall to create a vortex that propagates downstream (X-axis) and upwards (Y-axis) from the cavity.

From the initial study of the flow field caused by the presence of the cavity flameholder, as well as previous research by Allen (2005) and Gruber et al. (2001) it is clear that the fluid dynamics near the cavity are three-dimensional in nature. As will be discussed next, the addition of chemically reacting flow will further complicate the flow field. However, it is now possible to compare the results of reacting flow measurements

and calculations to those of the baseline case, with the ultimate goal being to discern the effects of adding combustion to the cavity flow field.

Reacting Flow:

In a combusting flow, a large amount of chemical energy is released into the flow. There are multiple variables that can be examined in order to ascertain the effects of the combustion process.

Static Temperature:

Often times the results of the energy release can be viewed in terms of increases in static temperature. Figure 25 below shows the static temperature distribution in the area of interest.

Figure 25. Static temperature distributions behind cavity ramp with flow out of page. Fuel injection rate is 32% and air injection rates are 0, 30, and 70%. Fuel and air percentages are to the right (F_X A_Y, X = %ethylene Y = %air). The color shading scheme is the same for all pictures.

There is an expected increase in temperature in moving from the baseline case to the first

combusting case (F_32 A_0). There is a core high temperature region located in the

center of the lobe structure found at $0.8 < Z < 2.2$ in. As air injection is increased from

30% (F_32 A_30) to 70% (F_32 A_70), the temperatures within the lobe structure

increase more than those in the surrounding areas. Increased air injection rates not only

grow the lobe region further out into the free stream, but also spread high temperature

near the tunnel floor farther into the main flow. Similar behavior is seen in Figure 26

with the higher fuel loading case (50% ethylene injection).

Figure 26. Static temperature distributions behind cavity ramp with flow out of page. Fuel injection rate is 50% and air injection rates are 0, 50, and 100%. Fuel and air percentages are to the right (F_X A_Y, X = %ethylene Y = %air). The color shading scheme is the same for all pictures.

Not surprisingly, with the higher fuel loading higher temperatures are seen throughout the area of interest, especially in the core area of the lobe structure. Growth of the high temperature regions into the free stream is fairly uniform. The spread is slightly more

uniform than was seen with the 32% fuel loading. An increase in maximum temperature

and temperature spread corresponds to increasing air injection levels.

Total Temperature:

The total temperature distribution is shown below in Figure 27.
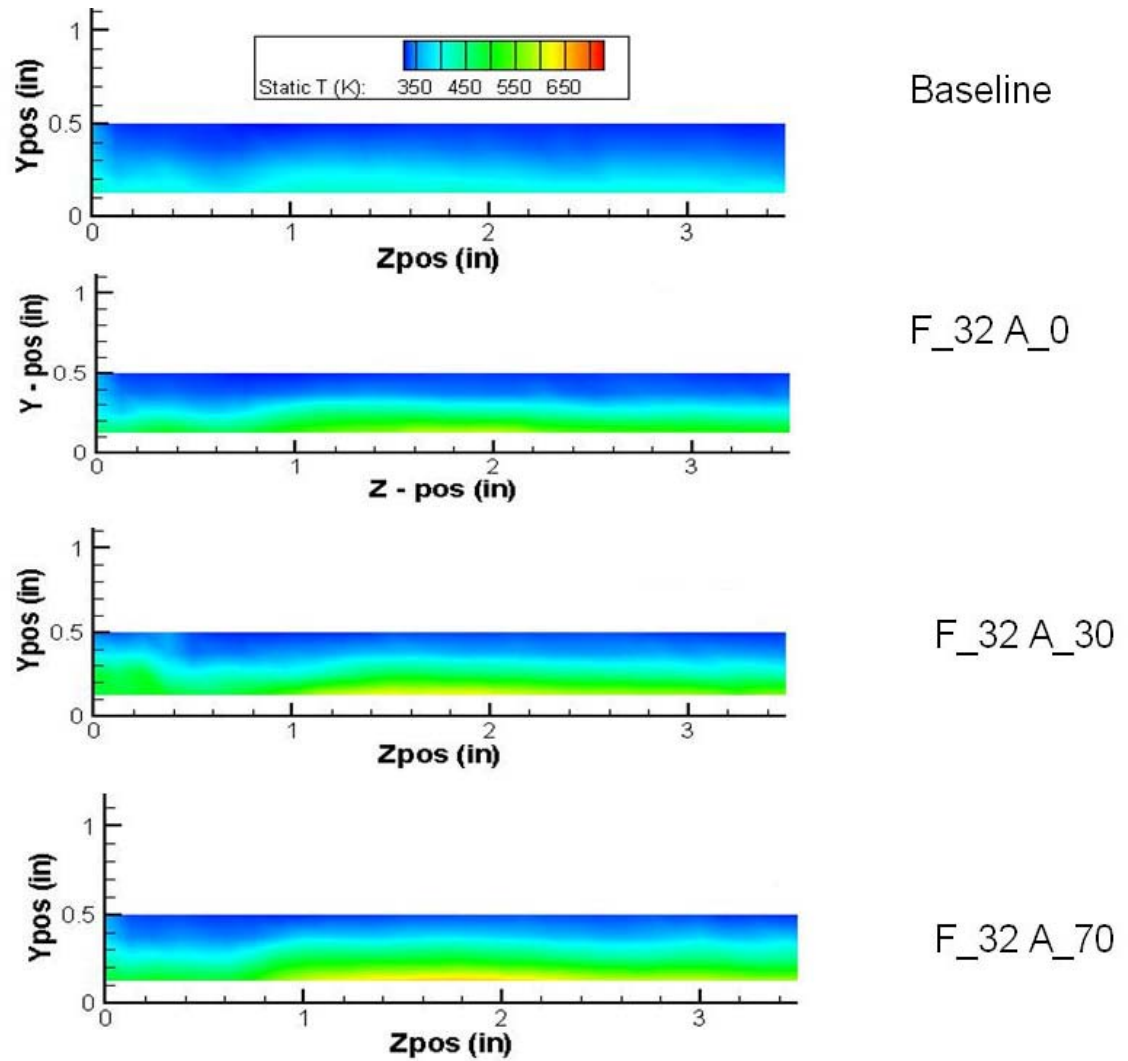

Figure 27. Total temperature distribution behind cavity ramp with flow out of
page. Fuel injection rate is 32% and air injection rates are 0, 30, and 70%. Fuel and air
percentages are to the left (F_X A_Y, X = %ethylene Y = %air). The color shading
scheme is the same for all pictures.

As with the static temperature distribution in Figure 25, the area of greatest increase in

total temperature is in the lobe structure. The gradients in the total temperature field

seem to be more concentrated around the lobe structure than with the static temperature.

Figures 25 and 26 show a fairly uniform spread across the lower bound of the area of

interest, whereas the contours in Figure 27 seem to hold the lobe shape farther into the

free stream flow. The addition of air injection did not change the general shape of the

total temperature distribution, but increasing the air injection rate did result in the

spreading of higher total temperatures vertically (Y-axis) into the free stream flow.

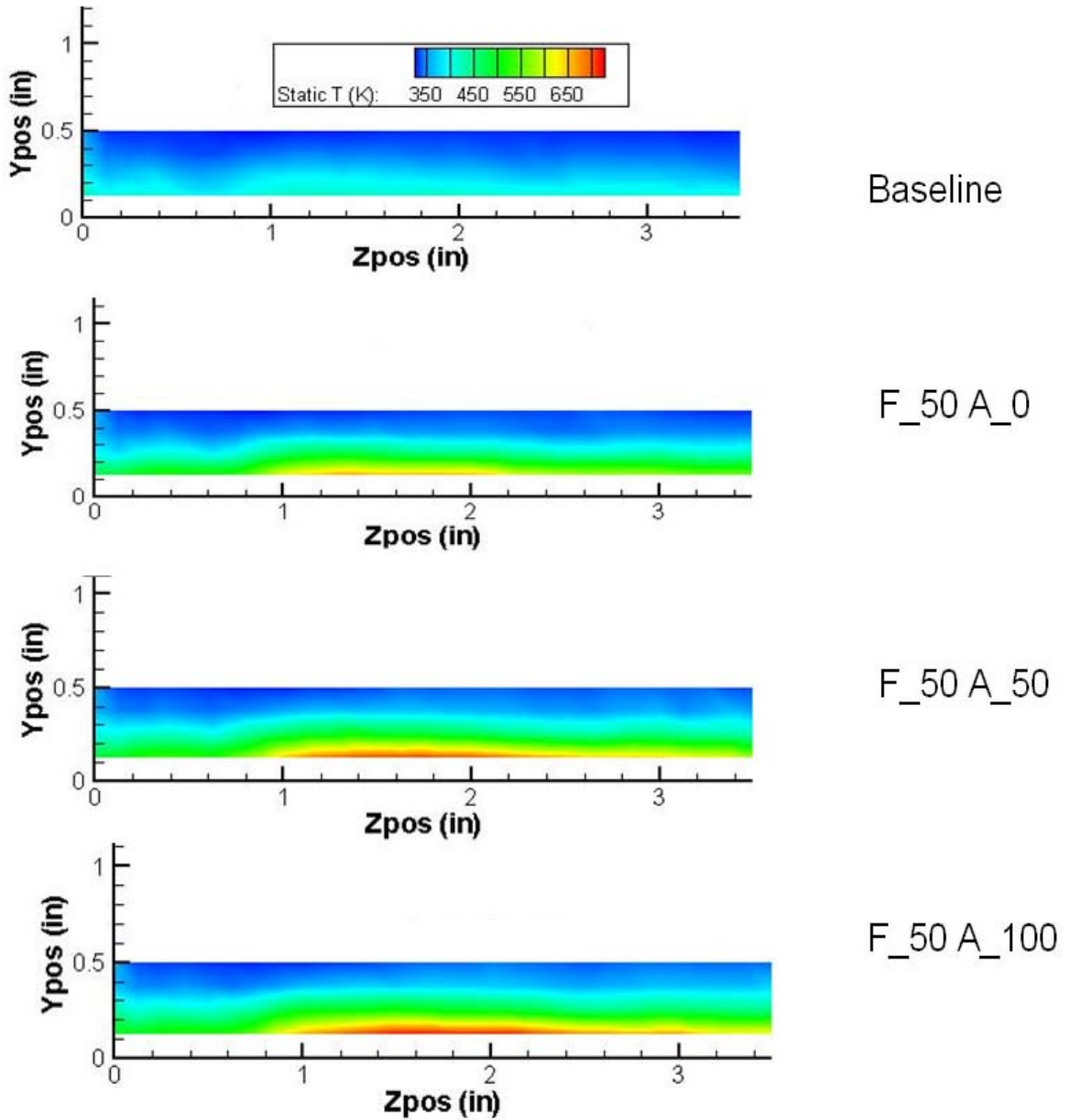Figure 28 shows the total temperature distribution for 50% ethylene injection.

Figure 28. Total temperature distributions behind cavity ramp with flow out of
page. Fuel injection rate is 50% and air injection rates are 0, 50, and 100%. Fuel and air
percentages are to the left (F_X A_Y, X = %ethylene Y = %air). The color shading
scheme is the same for all pictures.

As expected, the increases in total temperature were greater with the higher fuel loading.

The distribution of total temperature is more uniform about the lower bound of the area

of interest near the tunnel midspan, but the contours still hold the lobe shape as they approach the tunnel sidewall. The general shape of the distribution does not change with air injection, but the increasing air injection did result in higher total temperatures throughout the flow field, especially in the lobe structure.

Static Pressure:

There is also a rather expected increase in pressure resulting from the combustion process. As shown in Figure 29, a region of high pressure develops near the midspan line (3 in.) when combustion is established.

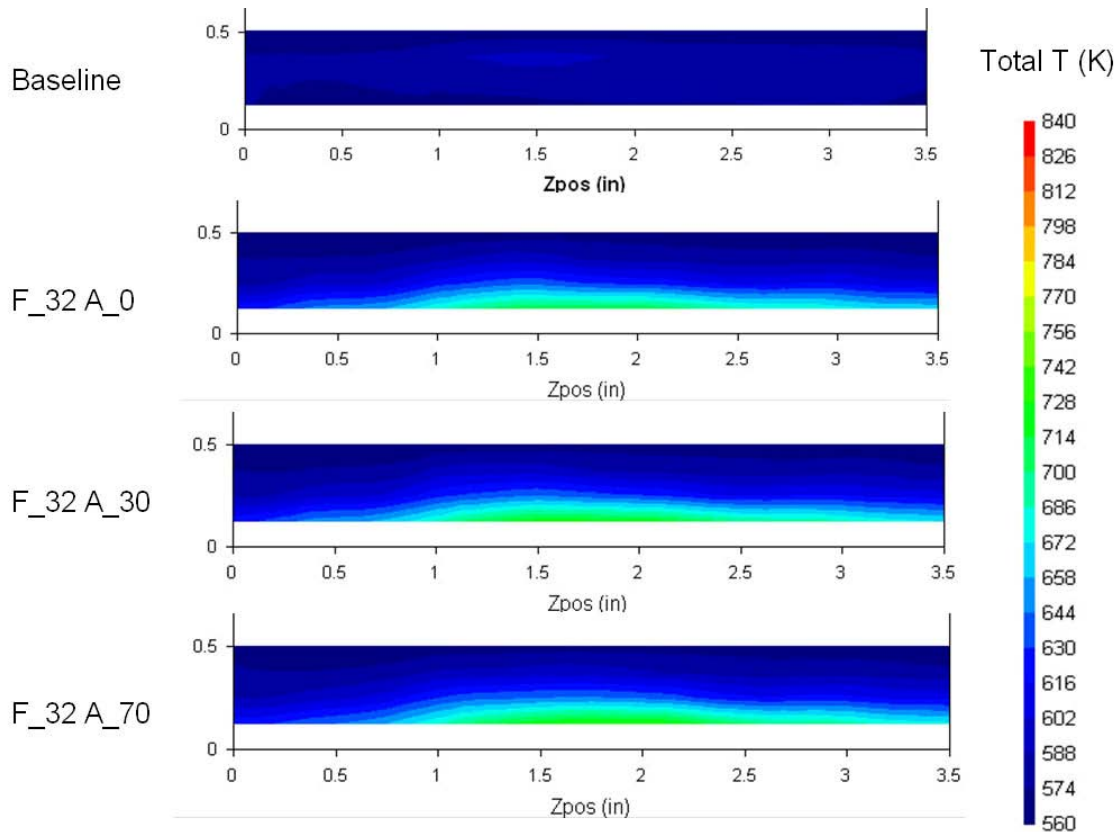Figure 29. Static pressure distributions behind cavity ramp with flow out of page. Fuel injection rate is 32% and air injection rates are 0, 30, and 70%. Fuel and air percentages are to the right (F_X A_Y, X = %ethylene Y = %air). The color shading scheme is the same for all pictures.

Increasing the air injection rate not only expands the high pressure region upwards into the free stream flow, but also spreads the region from the midspan line towards the sidewalls. Instead of a lobe structure located from $0.8 < Z < 2.2$ in., the region of highest pressure forms almost directly on the tunnel midspan line. Similar results can be

48

observed with the higher ethylene injection rates. Figure 31 shows the static pressure changes for the higher fueling cases.

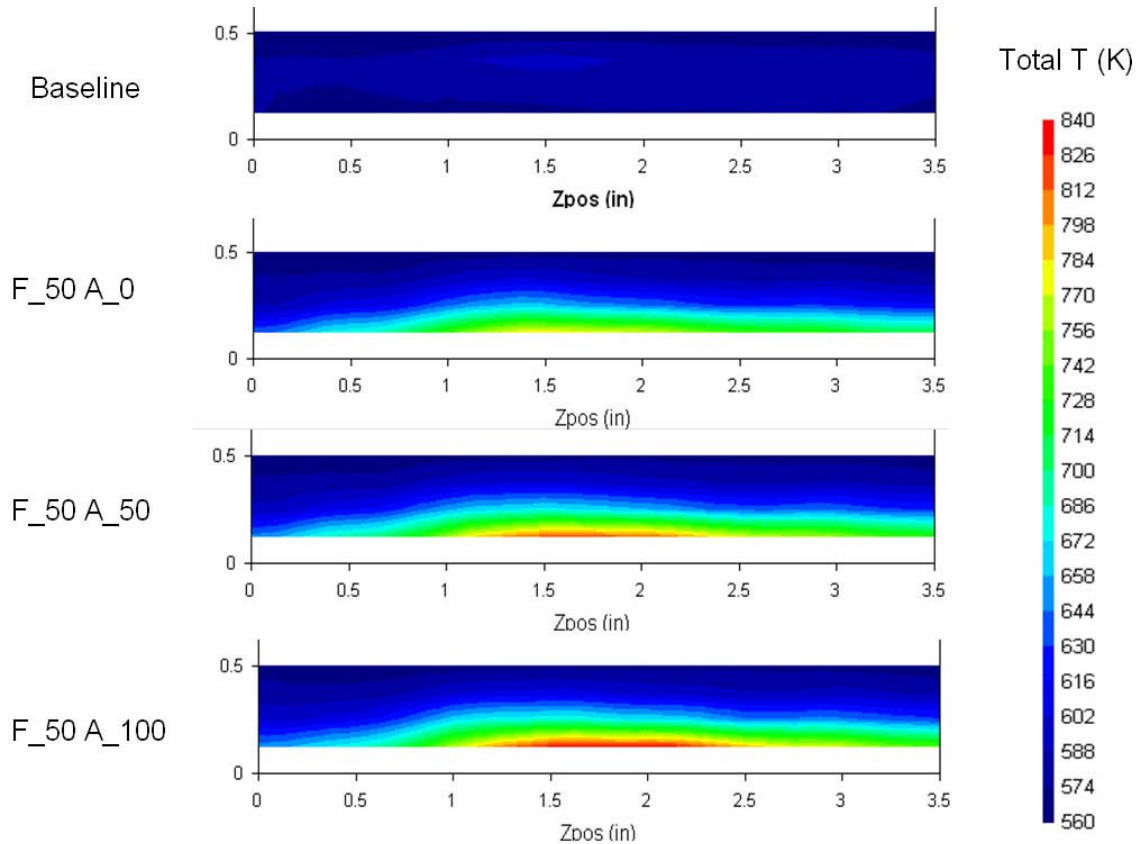Figure 30. Static pressure distributions behind cavity ramp with flow out of page. Fuel injection rate is 50% and air injection rates are 0, 50, and 100%. Fuel and air percentages are to the right (F_X A_Y, X = %ethylene Y = %air). The color shading scheme is the same for all pictures.

What is most notable with the higher ethylene injection rate is that the spreading of the high pressure region, both upwards into the free stream and laterally to the sidewalls, seems to be more complete with ethylene alone being injected. The addition of air

injection seems to increase the intensity and uniformity of the high pressure region. One area where continued spreading of high pressure with increasing air injection is observed is near the tunnel floor.

Mass Flux Distribution:

The spreading of high temperature and high pressure regions upwards into the free stream could be an indicator of the shear layer impinging farther up the cavity ramp. To better understand where the flow is actually concentrating in the area of interest, it is beneficial to examine the mass flux distribution. Figure 31 shows the mass flux distribution for 32% ethylene injection.
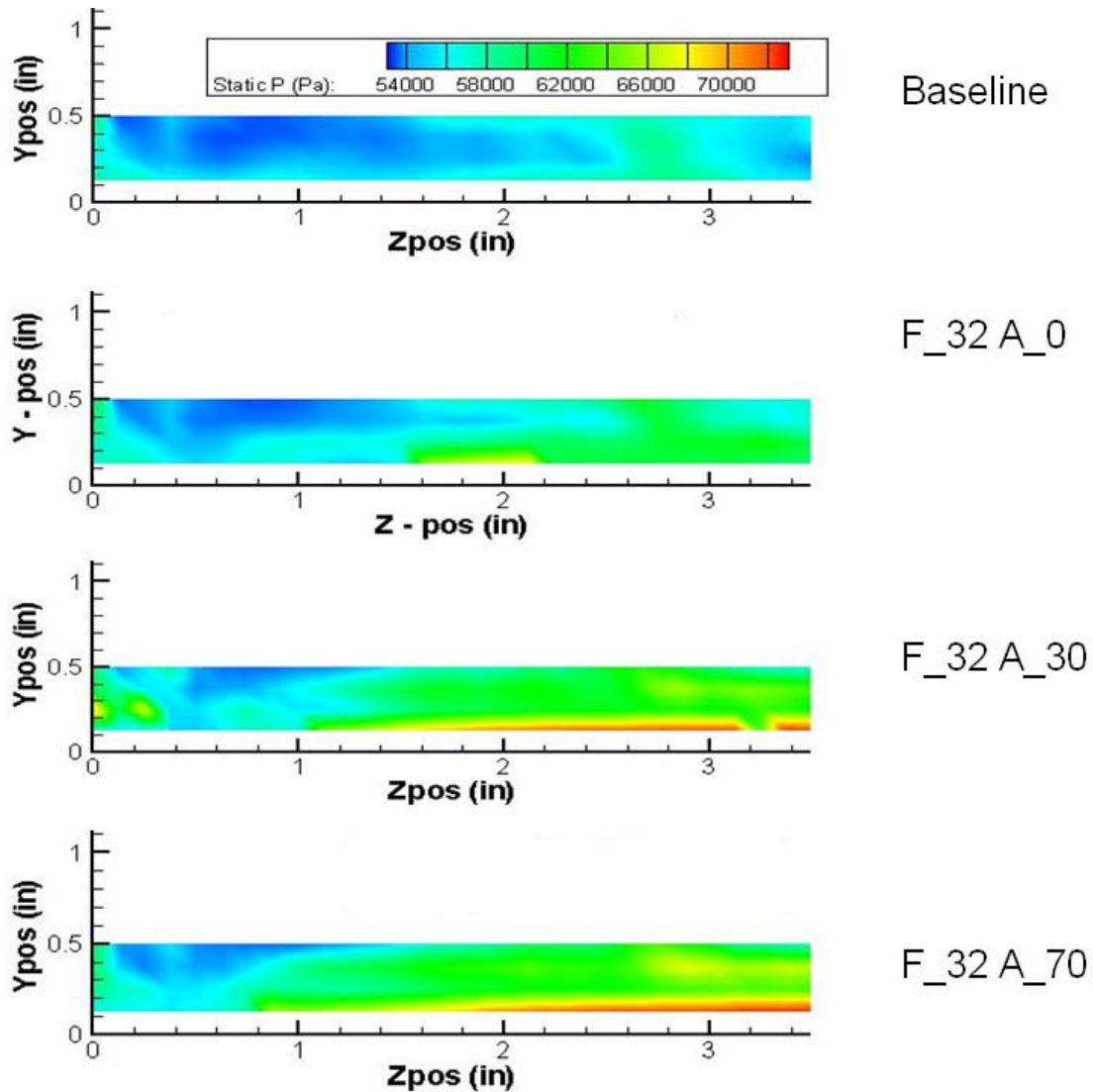
Figure 31. Mass flux distributions behind cavity ramp with flow out of page. Fuel injection rate is 32% and air injection rates are 0, 30, and 70%. Fuel and air percentages are to the right (F_X A_Y, X = %ethylene Y = %air). The color shading scheme is the same for all pictures.

It can be seen that the lobe area has a reduced amount of mass flux in comparison to the rest of the Z-axis. Increasing the air injection rate raises the area of reduced mass flux farther into the free stream. Figure 32 shows the mass flux distributions for the higher fuel loading.
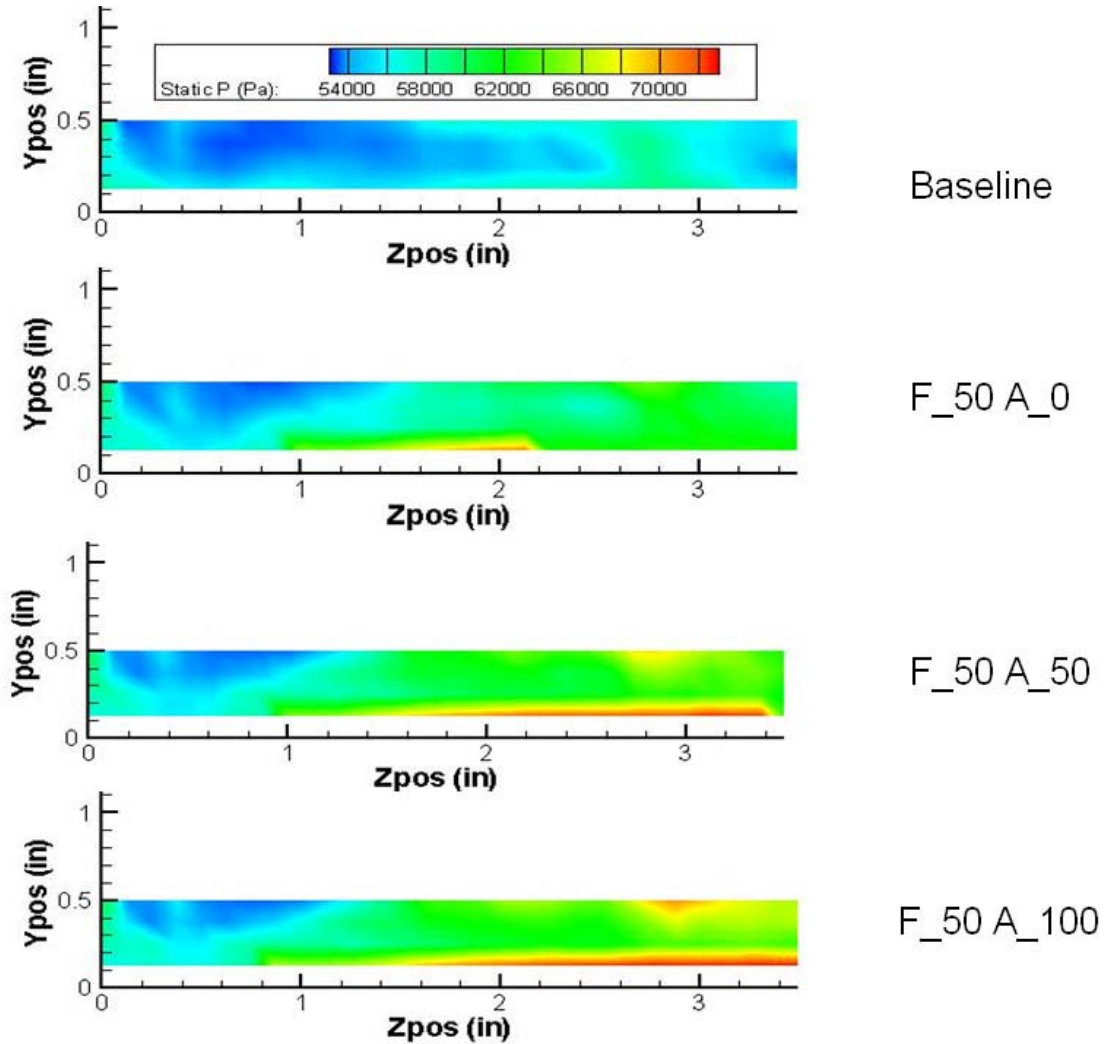
Figure 32. Mass flux distributions behind cavity ramp with flow out of page. Fuel injection rate is 50% and air injection rates are 0, 50, and 100%. Fuel and air percentages are to the right (F_X A_Y, X = %ethylene Y = %air). The color shading scheme is the same for all pictures.

The same general profile of reduced mass flux near the floor, concentrated around the lobe area, is seen with 50% ethylene injection. The addition of air injection seemed to have less effect on spreading reduced mass flux upwards into the free stream. The mass flux distributions, combined with the static temperature and pressure distributions seem to reinforce Allen's (2005) assertion that increased combustion caused by increased air injection leads to raising of the shear layer. The shear layer raising upwards causes the

lower bound of the supersonic free stream flow to raise upwards as well, decreasing the

mass flux through the area of interest.

Enthalpy:

An excellent way of determining if combustive heat release is being increased and

spread into the free stream flow, is to observe the changes in enthalpy. Enthalpy is a

measure of internal heat energy stored within any given unit of mass. Thus, enthalpy

shows where the combustion energy is released and transferred to the free stream flow.

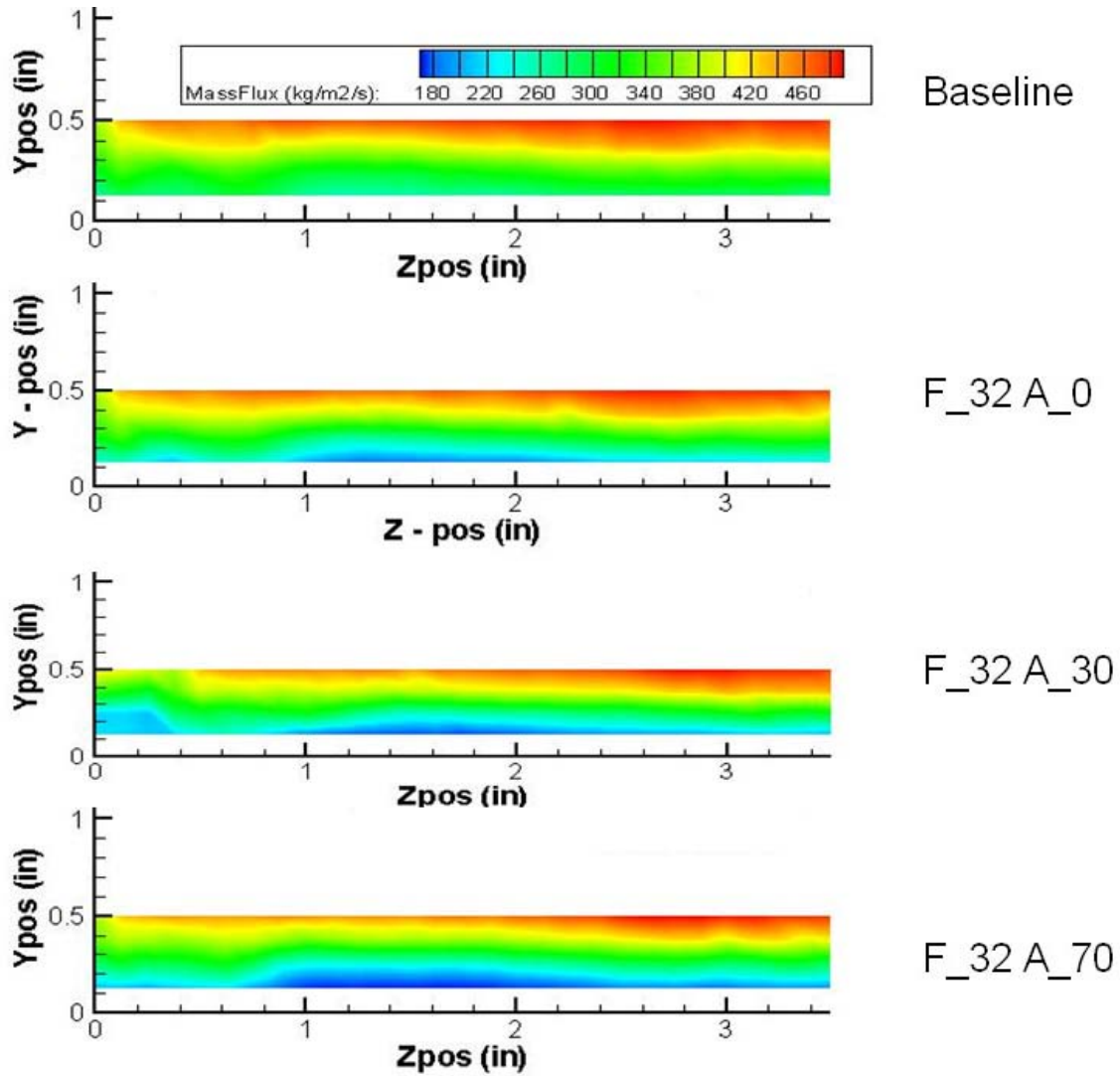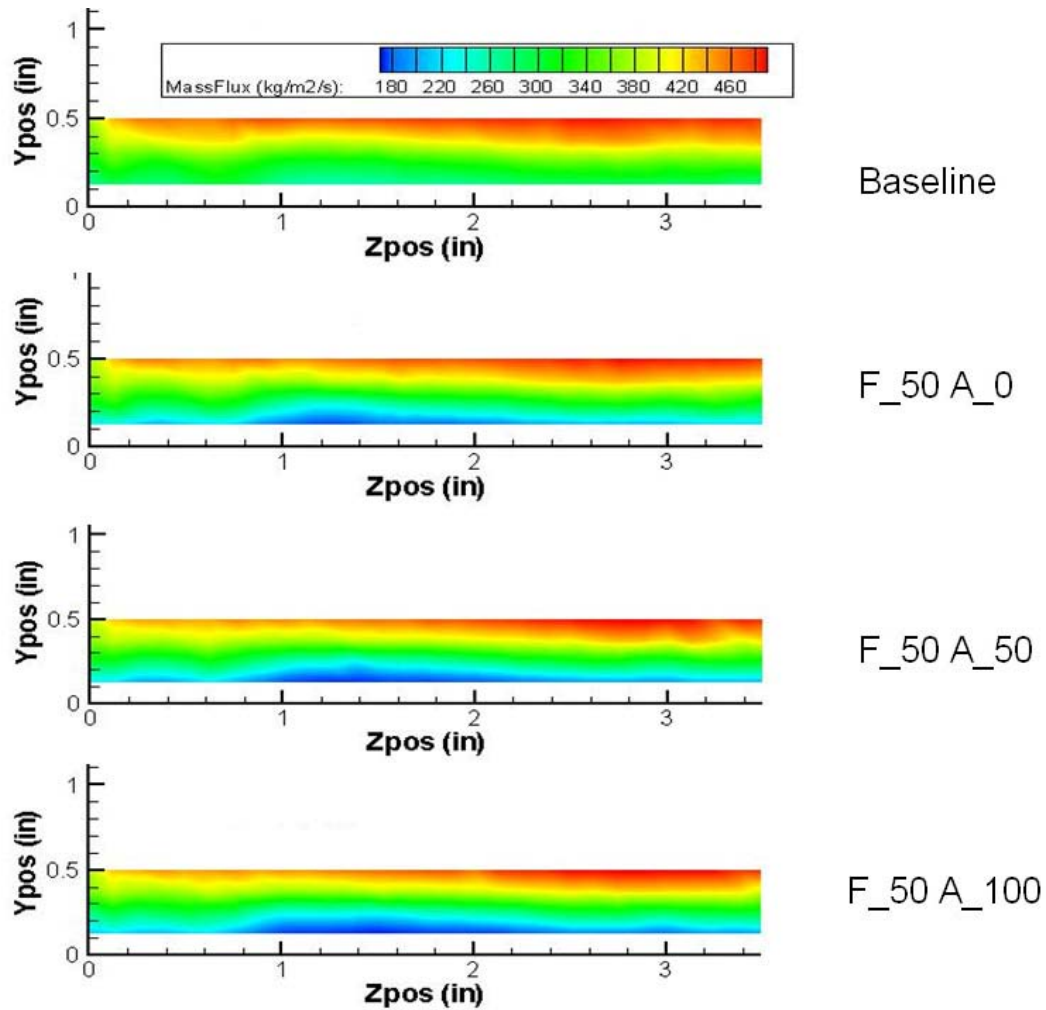Figure 33 shows the enthalpy distributions for the 32% ethylene injection rate.
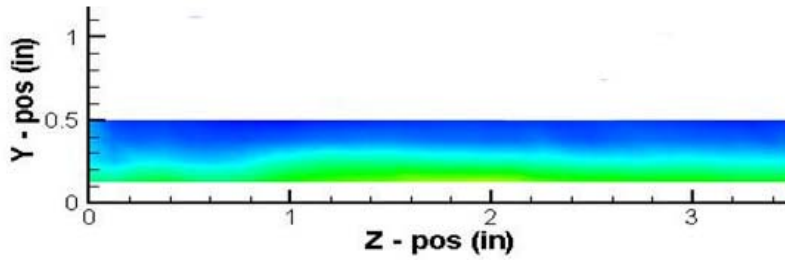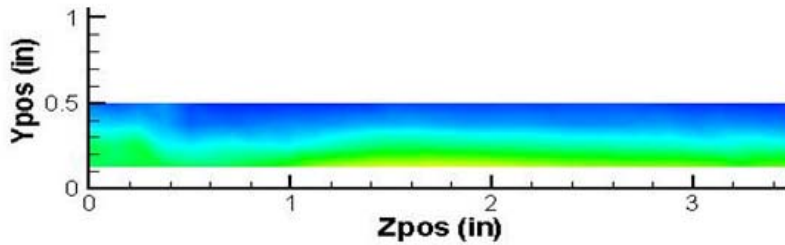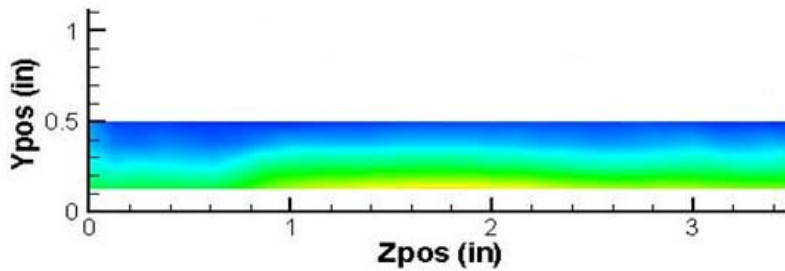
Figure 33. Enthalpy distributions behind cavity ramp with flow out of page. Fuel injection rate is 32% and air injection rates are 0, 30, and 70%. Fuel and air percentages are to the right (F_X A_Y, X = %ethylene Y = %air). The color shading scheme is the same for all pictures.

As expected, the contours of the enthalpy distributions closely resemble the contours of

the static temperature distributions. This is unsurprising, as Equation 20 defined static

enthalpy to be a function of static temperature alone. As mentioned in Chapter III,

enthalpy is not a linear function of temperature, due to the dependence of constant

pressure specific heat on static temperature. The nonlinearity of the enthalpy function will be most noticeable in high temperature areas, as the constant pressure specific heat experiences increases with the elevated temperatures. Obviously the most dramatic increase in enthalpy comes with the initial fuel addition and resulting combustion. Added air injection causes the enthalpy in the flow to gradually increase in both intensity and vertical penetration into the free stream. The enthalpy distribution for the 50% ethylene injection rate behaved similarly to the 32% case, as is seen in Figure 34.
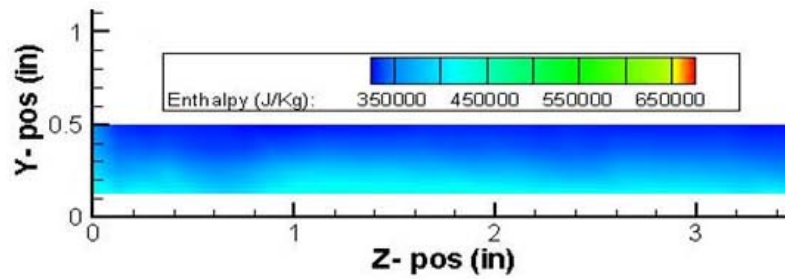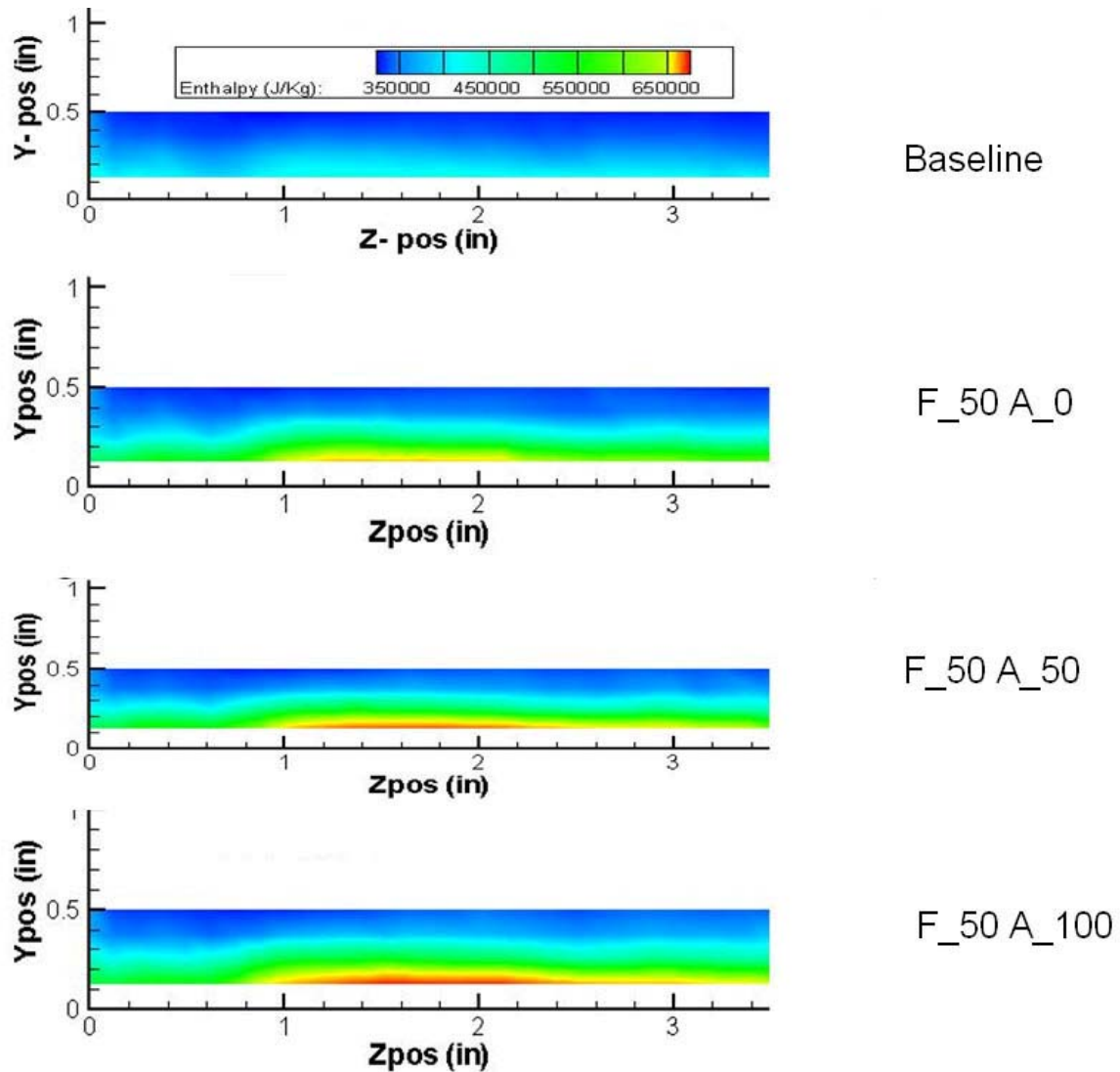
Figure 34. Enthalpy distributions behind cavity ramp with flow out of page. Fuel injection rate is 50% and air injection rates are 0, 50, and 100%. Fuel and air percentages are to the right (F_X A_Y, X = %ethylene Y = %air). The color shading scheme is the same for all pictures.

The increase in vertical spread of the region of increasing enthalpy was modest with increased air injection rates. The increase in intensity of enthalpy was more noticeable at the 50% fuel loading. Again the enthalpy distributions closely matched the static temperature distribution. Some slight discrepancies were seen with the 100% case.

These discrepancies came in the form of slightly different contour shapes. They occurred near the high temperature regions, for the fuel-air combination with the highest overall static temperatures, so the differences can most likely be attributed to the nonlinearity of the enthalpy function with respect to temperature. Figures 33 and 34 show an increase in enthalpy throughout the area of interest. The enthalpy values are higher and the enthalpy increase is spread out over a greater planar area with the addition of direct air injection.

In order to gain a better understanding of how increasing air injection affects the enthalpy gain in the area of interest it is beneficial to examine the gain in mass averaged enthalpy over the 0% air injection case. A mass weighted average for equally spaced points can be computed using equation 22 below.

$$\text{Mass Average Value} = [\sum (\text{Mass Flux})_i * (\text{Value})_i] / [\sum (\text{Mass Flux})_i] \qquad (22)$$

Table 2 shows the mass averaged values, as well as the normalized differences between them.

Table 2. Mass average enthalpy values comparison of cavity fueling schemes. Values of % increase are referenced to the fuel-only case for the respective fuel loading.

Fuel %	Air %	Mass Flux Avg. Enthalpy (J/Kg)	% Increase From 0% Air	Added Air Effectiveness
32	0	3.8E+05	N/A	N/A
32	30	4.0E+05	5.0	0.17
32	70	4.1E+05	6.2	0.089
50	0	4.0E+05	N/A	N/A
50	50	4.1E+05	4.1	0.081
50	100	4.2E+05	6.2	0.062

Clearly, from Table 2, increasing the amount of air injection increases the average enthalpy of the area of interest. Column 4 shows the percentage increase in enthalpy from 0% air injection for each fuel loading. The percentage increases were larger than

the estimated uncertainty of computed enthalpy, which was ±1.1% as stated in Appendix

B. Column 4 shows the percentage increase in average enthalpy (for initial air injection)

is greater for the lower fuel loading, but the increase in percentage enthalpy gain over the

0% air injection case is greater with the higher fuel loading. It is likely that the lower

fuel setting has received all of the enthalpy increasing benefits of air injection at a lower

air injection setting, and a diminishing gain effect is seen as air injection is increased

further. At the higher fuel loading, the full benefits of air injection are not realized until a

higher air injection % is used. Column 5 shows air injection effectiveness, which is the

ratio of percentage increase in enthalpy to the increase in air injection. Column 5 shows

that the ability of air injection to increase the enthalpy of the area of interest is greatest

for the lower fuel loading. Column 5 also shows that the benefits of increased air

injection begin to diminish at a lower air injection setting for the lower fuel loading.

Thus while air injection appears less effective at increasing combustive heat release at

higher fuel loadings on a per-unit-mass basis, the higher fuel loading appears to benefit

more from increasing air injection rate. That is the higher fuel loading stands to gain

more from increasing air injection, even if each unit mass of injected air effects the

higher fuel loading less than the lower fuel loading. It seems clear then that the air

injection method is directly affecting the cavity combustion by improving the fuel-air

mixture within the cavity, and thus leading to greater enthalpy spread into the area of

interest.

It is helpful to compare quantitative and qualitative data to gain a better

understanding of flow behavior. Allen (2005) performed multiple flow visualization

investigations for the same air injection scheme used in this research. Allen (2005) also

showed evidence of increased combustion being achievable by using air injection to improve the fuel-air mixture within the cavity, especially near the forward cavity step. Figures 35 and 36 show visual flame emission images from Allen's (2005) work.
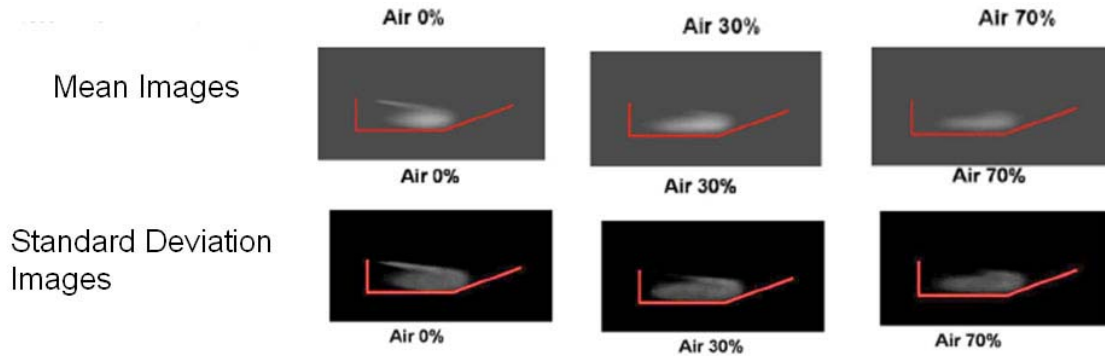
Figure 35. Luminous flame emission images for fuel loading of 32%. Red line is cavity geometry as viewed in the X-Y plane (Allen, 2005; used without permission).
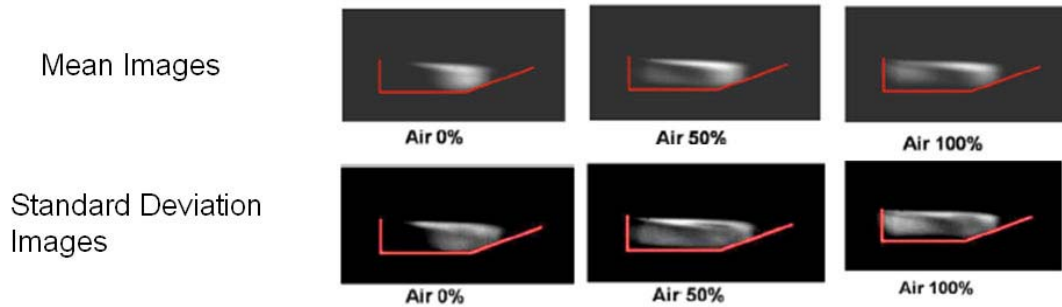
Figure 36. Luminous (visual) flame emission images for fuel loading of 50%. Red line is cavity geometry as viewed in the X-Y plane (Allen, 2005; used without permission).

In Figures 35 and 36, white areas indicate luminous (visual) flame emissions. Figure 35 reinforces the idea that, at the 32% fuel loading, the ability of air injection to improve combustion is maximized for a lower air injection setting, and that further increases in air injection lead to diminishing combustion increases. Figure 36 shows that at the higher fuel loading the air injection can be increased to nearly its maximum value while still seeing increases in luminosity, which is an indicator of combustive heat release. From Table 2 and Figures 35 and 36 it is clear that the ability of air injection to improve

combustion is based on its ability to modify the fuel-air mixture within the cavity. Thus the effectiveness of air injection in increasing combustion is highly dependent on the given fuel loading. Lower fuel loadings benefit from a lesser amount of injected air more than higher fuel loading. Higher fuel loadings can benefit from larger amounts of injected air more than lower fuel loadings. On a per-unit-mass basis air injection is less effective with the higher fuel loading, while the higher fuel loadings stands to gain more from larger increases in air injection. This is the ability of the air injection technique to tune the cavity for optimal performance.

Table 3 shows another point regarding the ability of air injection to increase enthalpy in the area of interest.

Table 3. Mass averaged enthalpy values reference base 32% fuel loading.

Fuel %	Air %	Mass Flux Avg. Enthalpy (J/Kg)	% Increase From 32% Fuel Only
32	0	3.8E+05	N/A
32	30	4.0E+05	5.0
32	70	4.1E+05	6.2
50	0	4.0E+05	4.0
50	50	4.1E+05	8.2
50	100	4.2E+05	10

Not only does the added injection of air increase the enthalpy over the 32% fuel-only combustion case, but even a modest amount of air injection, 30%, improves combustion more than simply increasing the fuel flow rate to 50%. Higher air injection rates show a greater increase in heat release over a simple increase in fuel loading. Table 3 shows that air injection can substitute for additional fuel to improve combustion and subsequent enthalpy spread into the area of interest. Since air can be bled from the core flow into the engine, albeit with some loss, fuel savings resulting from improvements in cavity

combustion efficiency can be realized by ensuring proper fuel-air mixing within the cavity flameholder through the use of direct air injection.

Total enthalpy shows the balance of the total flow energy between thermal and kinetic energies. Table 4 shows both the enthalpy and total enthalpy for the reacting flow cases.

Table 4. Mass averaged enthalpy and total enthalpy for reacting flow cases.

Fuel %	Air %	Mass Flux Avg. Enthalpy (J/Kg)	Mass Flux Avg. Total Enthalpy (J/Kg)	h/h_t
32	0	3.8E+05	6.1E+05	0.63
32	30	4.0E+05	6.1E+05	0.65
32	70	4.1E+05	6.1E+05	0.66
50	0	4.0E+05	6.2E+05	0.64
50	50	4.1E+05	6.3E+05	0.65
50	100	4.2E+05	6.4E+05	0.66

The change in fractional contribution to total enthalpy from thermal enthalpy with increased air injection occurred on the same order for both fueling cases. With the enthalpy ratio changing little as air injection is increased, it is reassuring to know that the chemical energy stored in the fuel is not being used to accelerate core flow, but rather to spread thermal energy into the free stream to aid in igniting main fuel mixed into the core flow. Accelerating the flow would further reduce the residence time of the flow through the combustor, which is undesirable.

Total Pressure:

Tunnel free stream total pressure was set to 80 psia (551600 Pa) for all experimental cases. Figure 37 shows the total pressure distribution for 32% fuel injection below.
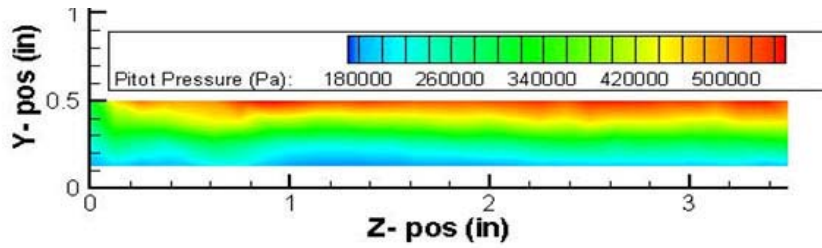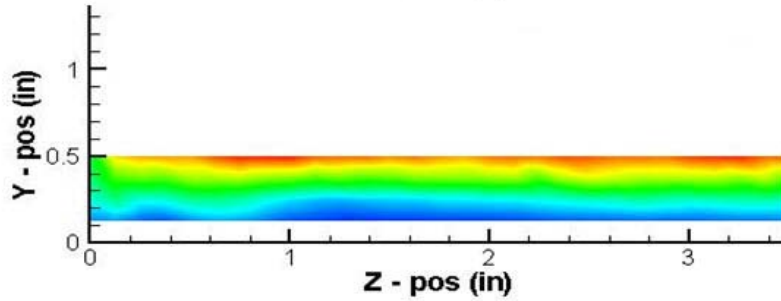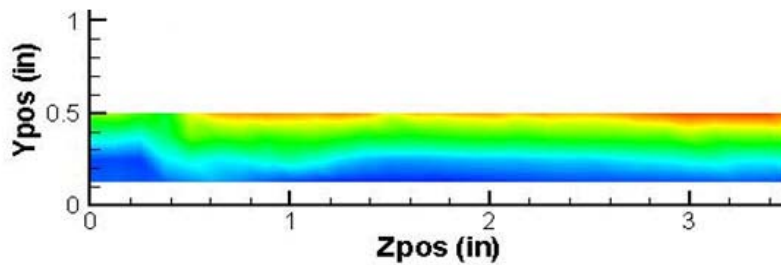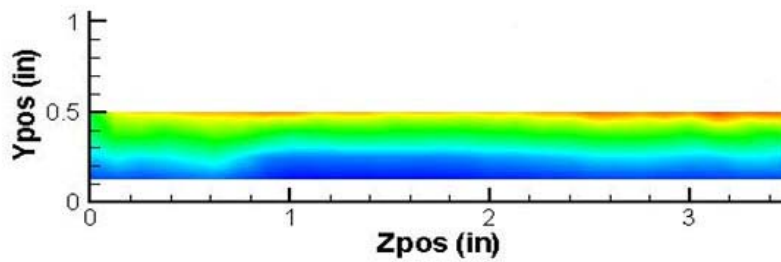
Figure 37. Total pressure distributions behind cavity ramp with flow out of page. Fuel injection rate is 32% and air injection rates are 0, 30, and 70%. Fuel and air percentages are to the right (F_X A_Y, X = %ethylene Y = %air). The color shading scheme is the same for all pictures.

As can be seen, the area of increased temperature and enthalpy corresponds to an area of

decreased total pressure. Total pressure losses increased as the air injection rate, and

resulting combustion and enthalpy spread, increased. The area of total pressure loss

extended upwards into the free stream with increasing air injection. The general shape of

the total pressure contours remained the same throughout the range of air injections rates.

Figure 38 shows the total pressure distribution for 50% ethylene injection.
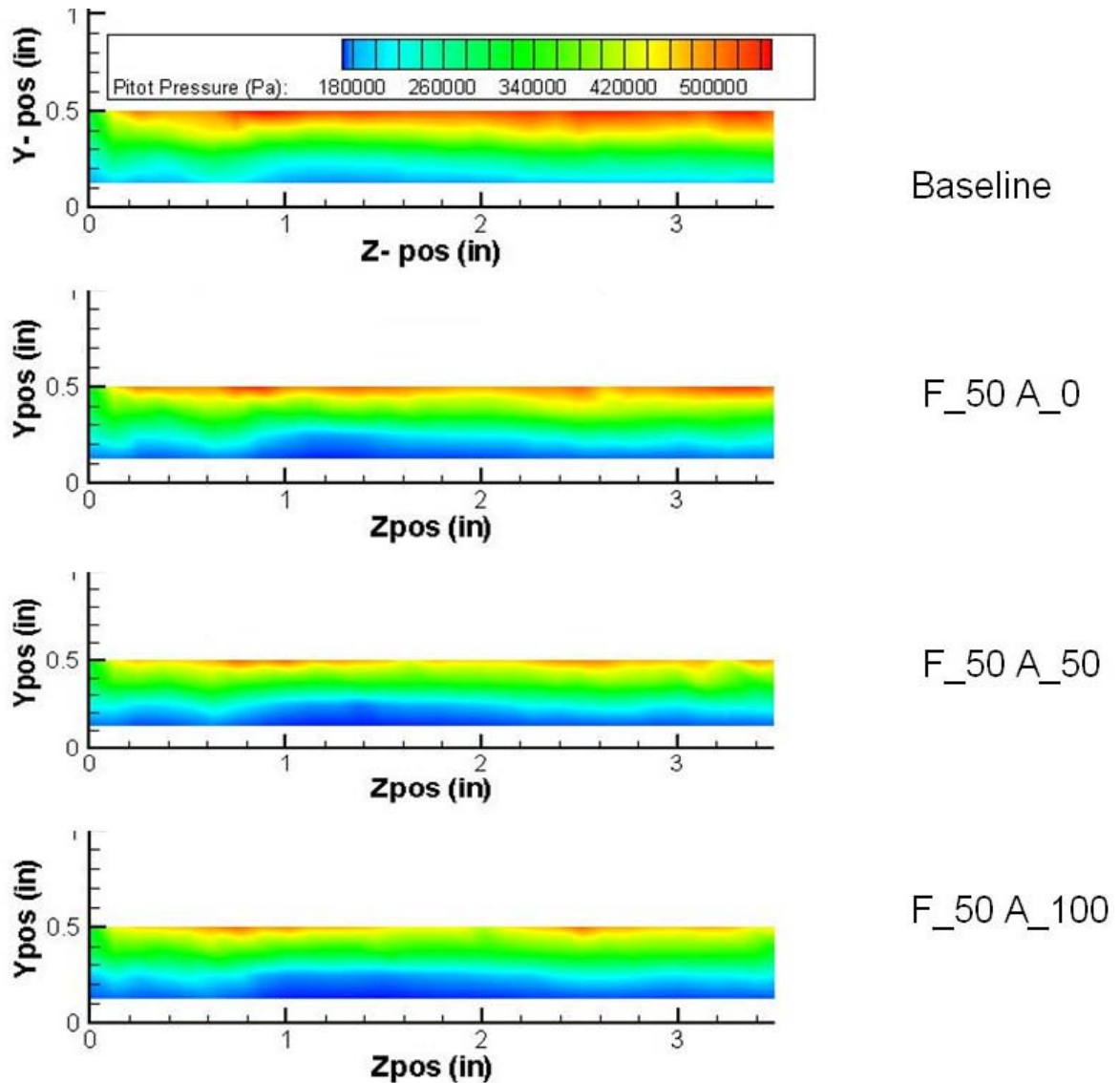
Figure 38. Total pressure distributions behind cavity ramp with flow out of page. Fuel injection rate is 50% and air injection rates are 0, 50, and 100%. Fuel and air percentages are to the right (F_X A_Y, X = %ethylene Y = %air). The color shading scheme is the same for all pictures.

Again the areas of decreased total pressure correspond to the areas of increased

temperature and enthalpy. The total pressure contours for the 50% fuel case closely

match the contours for the 32% case, with the area of reduced total pressure being slightly greater in the 50% case. This corresponds to the higher enthalpy and temperature spread into the free stream by the 50% case.

Total pressure losses result in undesirable, but unavoidable, thermodynamic cycle inefficiencies. A common presentation of total pressure losses is the normalized difference from the free stream value. For this research the free stream value was set to be 80 psia (551600 Pa). Data taken at a Y-axis value of 1.0 in yielded a mass average total pressure of 79.5 psi (548000 Pa). The tunnel height (Y-axis) at the probe streamwise location was approximately 2.5 in. Thus it is safe to assume the tunnel free stream setting of 80 psi applies to the tunnel free stream flow, and can be used as a reference value for determining total pressure losses. Normalizing the total pressure difference presents the data as a fraction of the total pressure in the free stream, with 0 (no loss) representing free stream conditions. Table 5 shows the normalized total pressure loss and the percentage difference between the various experimental cases.

Table 5. Mass averaged total pressure losses.

Fuel %	Air %	Normalized Mass Flux Avg. P_o Loss	% Increase From Baseline	% Increase From 32% Fuel 0% Air	% Increase From 0% Air
0	0	0.32	N/A	N/A	N/A
32	0	0.36	11	N/A	N/A
32	30	0.41	27	14	14
32	70	0.42	29	16	16
50	0	0.37	14	2.8	N/A
50	50	0.40	23	11	7.7
50	100	0.41	27	14	11

As can be seen there are significant total pressure reductions, from free stream conditions, associated with the mere presence of the cavity in the combustor. The area of

interest covers approximately 20% of the total combustor area at that streamwise location (assuming spanwise symmetry). The total pressure losses were greatest in and immediately below (Y-axis) the area of interest, and the total pressure losses decreased while moving farther into the free stream. Thus the normalized total pressure losses throughout the entire combustor will be lower than those reported for only the area of interest.

Column 4 of Table 5 shows the percentage increases for total pressure losses over the area of interest. The estimated uncertainty for the normalized total pressure losses is estimated to be ±2.8%, as described in Appendix B. The percentage increases in Column 4 for the lower fuel loading are less than this uncertainty, but the increases for the higher fuel loading are greater than the estimated uncertainty. Since the changes in total pressure loss behave similarly for both fuel loadings and the changes for the higher fuel loading cases were outside the uncertainty margin, it is not unreasonable to assume the percentage increases for the lower fuel loading cases are real increases and not data scatter. Column 3 shows the increases in total pressure loss from fuel and air injection are fairly small, relative to the losses associated with the cavity itself. Column 3 also shows that while the initial amount of air injection resulted in total pressure loss increases of the same order as those associated with the addition of fuel only, further increases in air injection resulted in diminishing increases in total pressure loss. What is also interesting about column 3 is that the total pressure losses experienced with the higher fuel loading with added air injection were equal to, if not less than those with the lower fuel loading with added air injection. This occurs while the higher fuel loadings yields

larger enthalpy increases. This initially indicates that air injection is most effectively used with higher fuel loadings, from a perspective of minimizing loss.

To better see the effect of air injection alone on total pressure loss it is helpful to examine column 6 of Table 5. The percentage differences in column 6 are referenced to the fuel-only case for each respective fuel loading. Thus the values represent changes resulting only from increasing air injection rates for a given fuel loading. From column 6 it is clear that the relative increases in total pressure loss resulting from air injection are greater with the lower fuel loading, but the rate at which those losses increase with additional air injection is less than the rate of increase with the higher fuel loading. This is similar to the behavior of combustive heat release seen in Table 2. For the 32% fuel setting, there was a larger initial increase in total pressure loss, followed by diminishing pressure loss increases mirrors the behavior of the enthalpy. The higher fuel loading case showed smaller initial increases in total pressure loss while experiencing larger increases as air injection was increased. In considering column 5, one can see that injecting additional fuel alone from the reference condition of 32% fuel alone resulted in the smallest increase in total pressure loss. The increases in total pressure loss were lower with the higher fuel loading, but were also shown to be increasing at a faster rate. This again shows that higher fuel loading case was beginning to be affected by the air injection technique at a higher air injection rate than the lower fuel loading.

With enthalpy gains and total pressure losses behaving in much the same way for each respective fuel setting, a cost-benefit effect resulting from increased air injection can be observed by examining the ratio of the percentage increase in enthalpy to the percentage increase in total pressure losses. Table 6 shows the cost-benefit effects.

Table 6. Costs and benefits of increasing air injection.

Fuel %	Air %	% Increase in Po Loss From 0% Air	% Increase in Enthalpy From 0% Air	Benefit--Cost Ratio
32	0	N/A	N/A	N/A
32	30	14	5.0	0.37
32	70	16	6.2	0.39
50	0	N/A	N/A	N/A
50	50	7.7	4.1	0.53
50	100	11	6.2	0.54

It is immediately evident that for both fuel loadings, regardless of air injection rate, the percentage increase in total pressure losses outweighs the percentage gains in enthalpy. However, increasing the air injection rate does improve the Benefit – Cost Ratio slightly. The ratios are significantly greater for the higher fuel loading. Again it seems that the lower fuel loading is aided by air injection less than the higher fuel loading. This would be consistent with the idea that the combustion efficiency of the higher fuel loading is reduced more by the increasingly fuel-rich vortex trapped near the cavity's forward step. Table 7 below is similar to Table 6, but the values in Table 7 are referenced to the 32% fuel only case. If one considers 32% fuel only to be the baseline operating condition, Table 7 reveals the best way to gain as much increase in enthalpy spread for the least amount of increase in total pressure loss.

Table 7. Costs and benefits of increasing air injection.

Fuel %	Air %	% Increase in Po Loss from 32% Fuel Only	% Increase in Enthalpy from 32% Fuel Only	Benefit--Cost Ratio
32	0	N/A	N/A	N/A
32	30	14	5.0	0.37
32	70	16	6.2	0.39
50	0	2.8	4.0	1.4
50	50	11	8.2	0.76
50	100	14	10	0.72

Column 5 of Table 7 demonstrates again that direct air injection is most effectively used at higher fuel settings, since the Benefit-Cost Ratio is greater for the higher fuel loading cases. Obviously the best way to increase enthalpy without increasing the total pressure loss is to simply increase the fuel injection rate. Since air can be bled from the core atmospheric flow through the engine it is desirable to use air injection rather than fuel (which must be stored) to improve the performance of the combustor.

Gas Analysis:

The gas analyzer measured concentrations of oxygen (O_2), carbon monoxide (CO), hydrocarbons (C_xH_y), and nitrous oxides (NO_x). The gas analyzer receives dry samples (the incoming gas passes through a desiccator).

In investigating the effectiveness of direct air injection at improving cavity combustion, it is helpful to examine the changes in O_2, C_xH_y, and NO_x concentrations. A drop in O_2 concentration will indicate that combustion has taken place. A similar investigation could be done with the increase in CO emissions, but the contours for CO production and O_2 depletion were nearly identical, and will not be presented here. The presence of C_xH_y could mean that some fuel was not combusted and was transported into the free stream, or it could mean that the reaction is slow and is spreading down stream with the probe measuring not unburned fuel, but intermediary C_xH_y species such as CH_3. The formation of NO_x compounds is also indicative of combustion. The formation of NO_x compounds is maximum at higher temperatures, and thus it is to be expected that NO_x concentrations will be higher for fuel-air settings that produced higher temperatures. Since the probe tip is approximately 2.25 in aft of the cavity exit, the probe will see the

free stream flow to a large extent, and thus the changes in O_2 concentration will not be commensurate with levels typically expected from complete combustion. Gas mixture concentration changes will be diluted by the free stream flow, since the probe is measuring the combustion products carried down stream by the free stream.

Figure 39 shows the distribution of O_2 concentration for 32% fuel loading.

Figure 39. Oxygen concentration behind cavity ramp with flow out of page for 32% ethylene. Fuel and air percentages are to the left (F_X A_Y, X = %ethylene Y = %air).

A lobe of reduced oxygen concentration is noticeable in the same location as the combustion lobe that was present in numerous other figures. Also of note is that the maximum decrease in oxygen concentration was only 1.3%. This demonstrates that gas mixture changes seen by the probe tip will be small throughout this analysis. Increasing

air injection from 0% to 30% seems to have minimal effect, but increasing air injection

from 30% to 70% appears to spread the region of reduced O_2 concentration upwards into

the free stream and reduce the width of the base of the lobe with the greatest degree of

oxygen reduction. Figure 40 presents the O_2 concentrations for the 50% fuel loading.
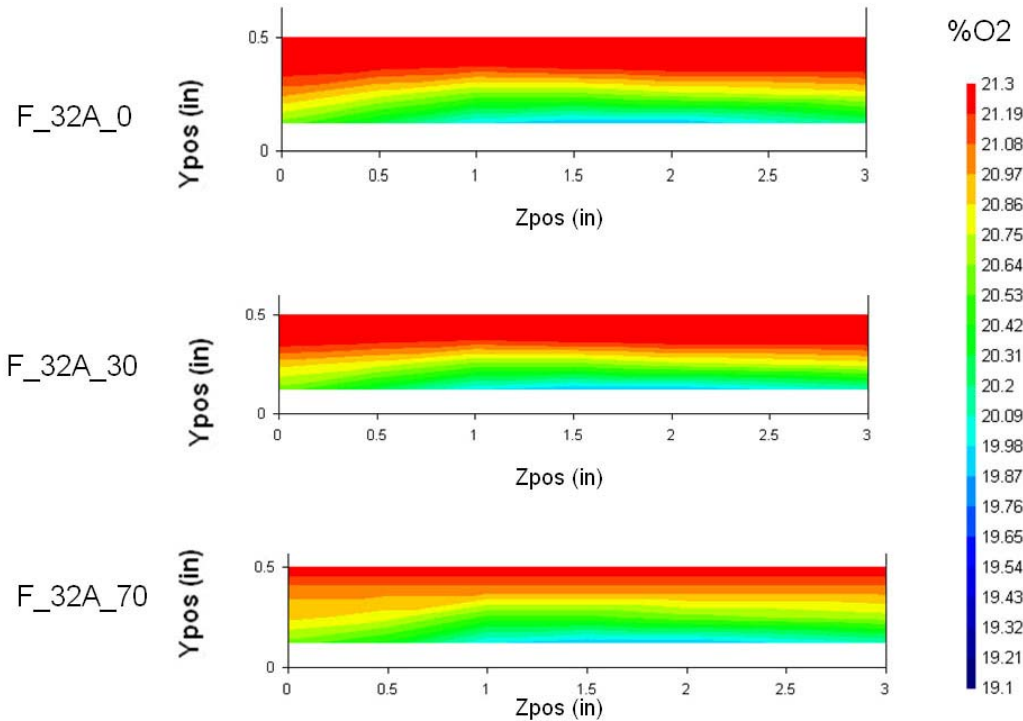

Figure 40. Oxygen concentration behind cavity ramp with flow out of page for
50% ethylene. Fuel and air percentages are to the left (F_X A_Y, X = %ethylene Y =
%air).

Not surprisingly, the amount of oxygen depletion (2.2% maximum) was greater for the

higher fuel loading. The general shape of the O_2 distribution is the same as with the

lower fuel setting. Increasing air injection resulted in further depletion of oxygen in the

lobe core. Air injection, as with the 32% fuel loading, stretched the O_2 reduction area

upwards and shrank it spanwise to a small degree.

Concentration of hydrocarbons typically shows unburned fuel escaping the combustion reaction. Figure 39 shows the hydrocarbon distribution for 32% ethylene injection.

Figure 41. Hydrocarbon concentration behind cavity ramp with flow out of page for 32% ethylene. Fuel and air percentages are to the left (F_X A_Y, X = %ethylene Y = %air).

Unburned hydrocarbons seem to escape the cavity in a series of plumes. With no air injection there is significant escape of unburned hydrocarbons. Adding air injection (0-30%) improves the fuel air mixture and results in improved combustion and fewer unburned hydrocarbons. However, further increases in air injection (30-70%) results in a large increase in unburned hydrocarbons. The increase could be due to the addition of excess air that makes the cavity mixture too lean for efficient combustion. The idea that

too much air injection, particularly for the lower fuel setting, would lead to diminishing

gains in combustion has been expressed earlier (see Table 2, column 4), and Figure 39

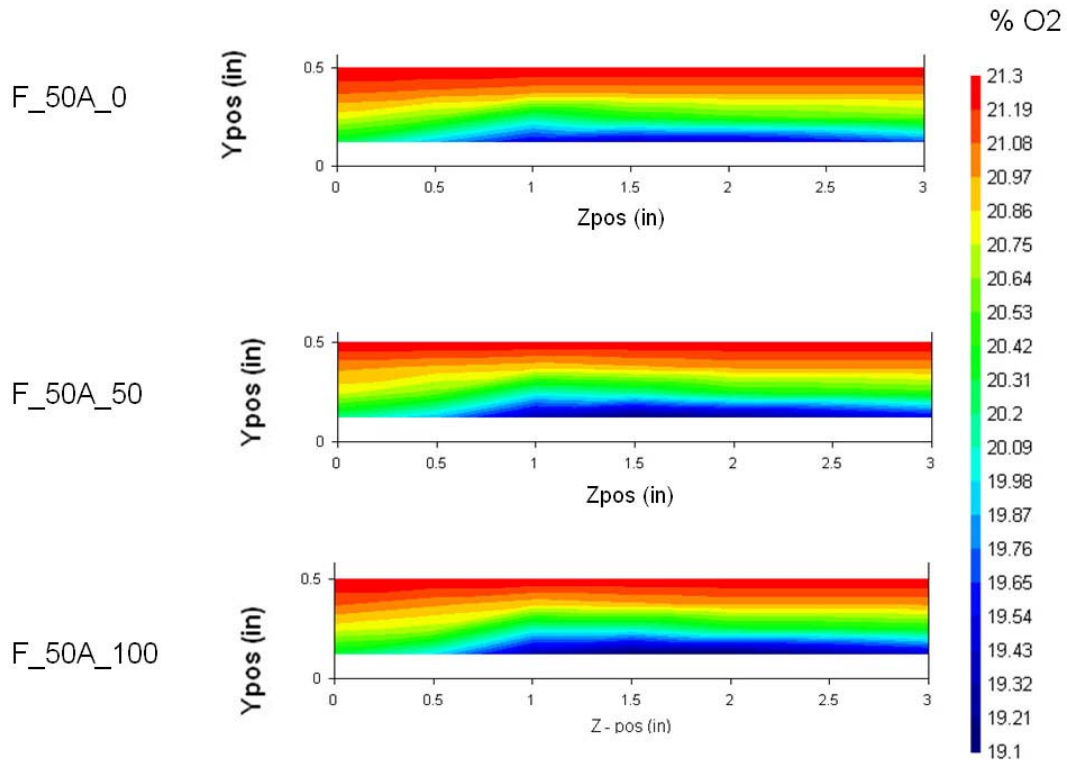seems to agree. Figure 42 shows the C_xH_y concentrations for the 50% fuel loading.
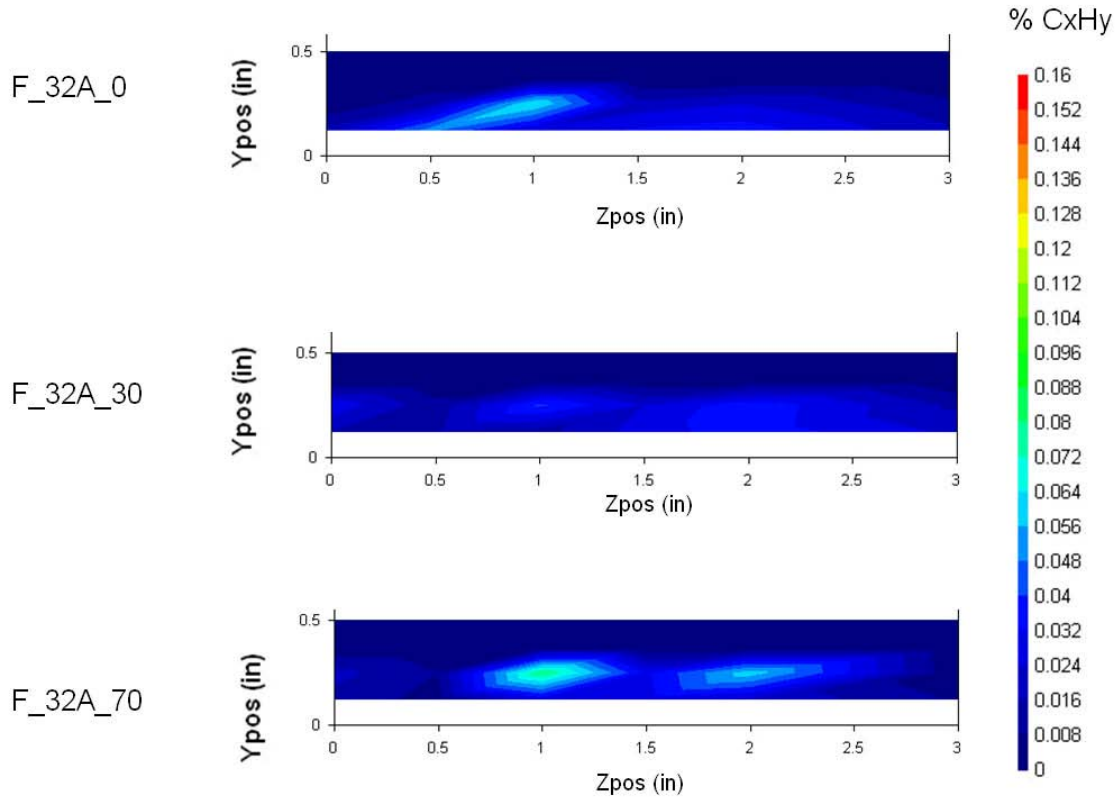

Figure 42. Hydrocarbon concentration behind cavity ramp with flow out of page
for 50% ethylene. Fuel and air percentages are to the left (F_X A_Y, X = %ethylene Y =
%air).

The distribution of unburned hydrocarbons is more uniform about the area of interest for

the higher fuel setting. Higher amounts of hydrocarbons are detected for the higher fuel

loading, especially with no air injection. Adding air injection continually improves the

cavity combustion of the 50% fuel loading, as evidenced by steady reductions in

unburned hydrocarbons resulting from increased air injection. This agrees with previous

figures showing air injection to be beneficial for improved combustion with the 50% fuel

72

loading up to the 100% air injection level. The air injection does not reach a level that

causes the cavity mixture to become too lean for combustion at the higher fuel loading.

Production of nitrous oxides (NO_x) is another indicator of combustion. Since

NO_x formation is greatest at higher temperatures, NO_x concentrations indicate

combustion weighted by thermal energy released by the reaction. Figure 43 shows the

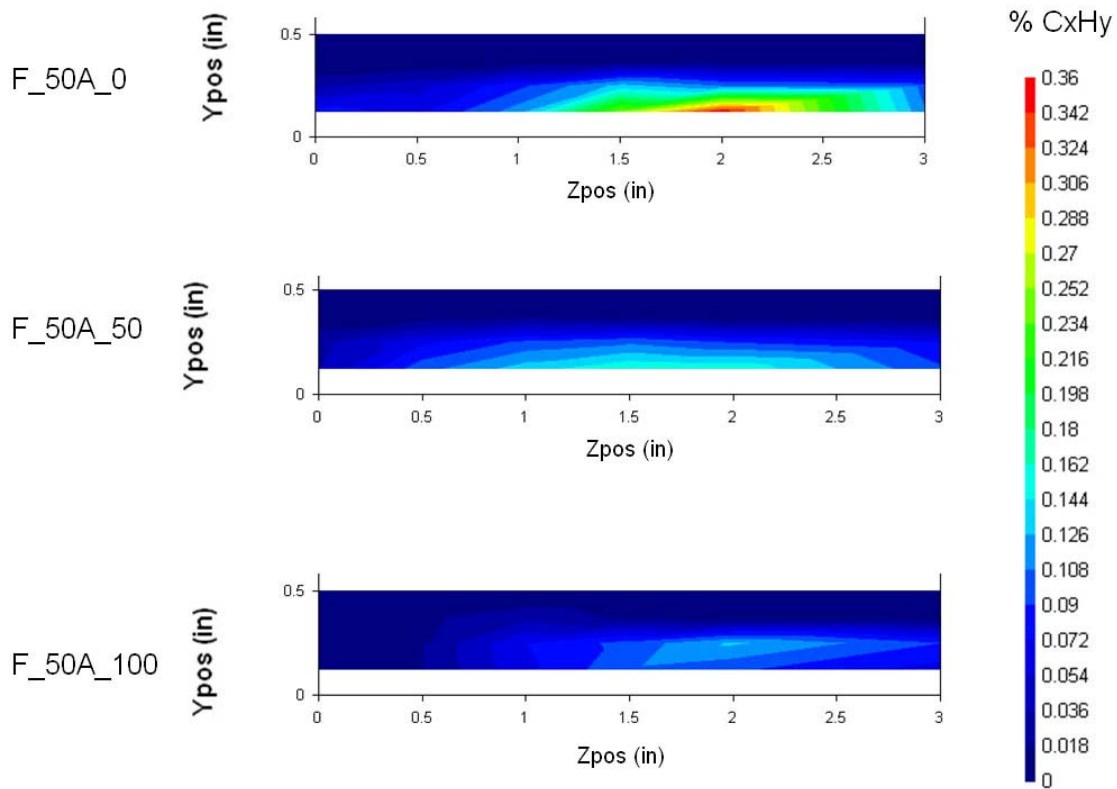nitrous oxide distribution for 32% ethylene injection.

Figure 43. Nitrous oxide concentration behind cavity ramp with flow out of page
for 32% ethylene. Fuel and air percentages are to the left (F_X A_Y, X = %ethylene Y =
%air).

The first thing to glean from Figure 43 is that the concentrations of nitrous oxide were

low for all cases. Nitrous oxide formation increases with air injection, although the

increase is greater for 70% air injection than for 0% or 30% air injection. Increases in

NO_x formation is greatest in the core of the combustion lobe, where the temperature is greatest (as shown in Figure 25). Figure 43 shows the NO_x concentration farther into the free stream seemed to decrease with air injection. Thus in combining increased NO_x production in the high temperature lobe and decreased NO_x production nearer the free stream, the net effect is a slight change in NO_x production for 70% air injection, which agrees with the lack of O_2 reduction and the increase in unburned hydrocarbons that was seen in Figures 39 and 41, respectively. Figure 44 shows NO_x concentration distributions for 50% ethylene injection.
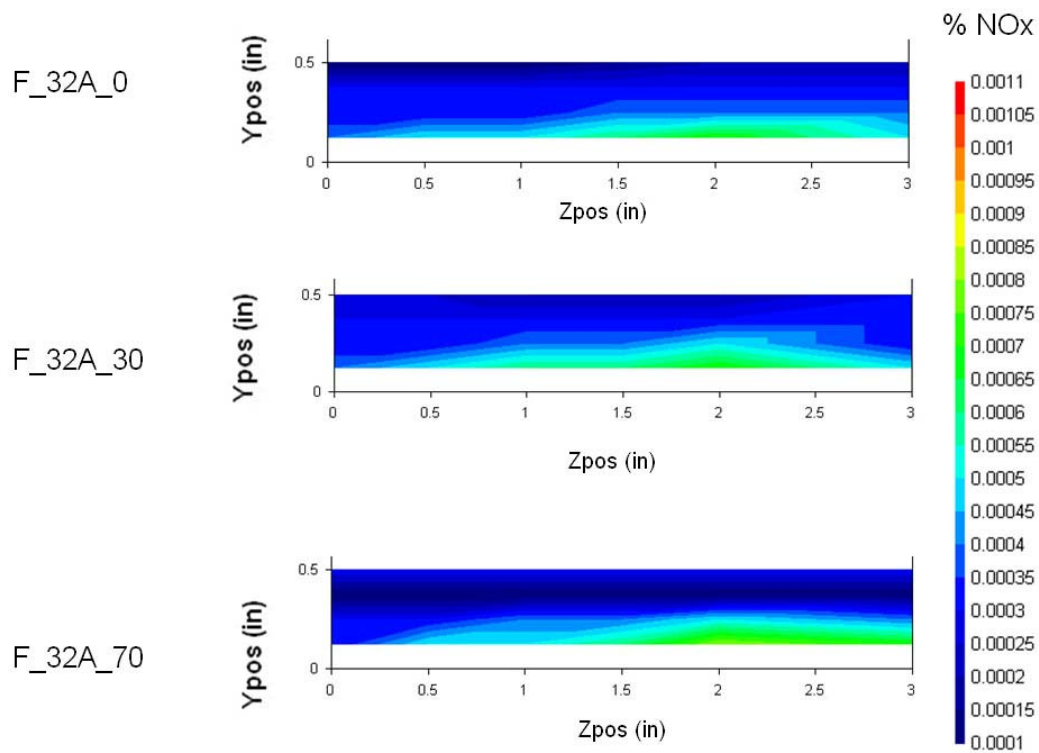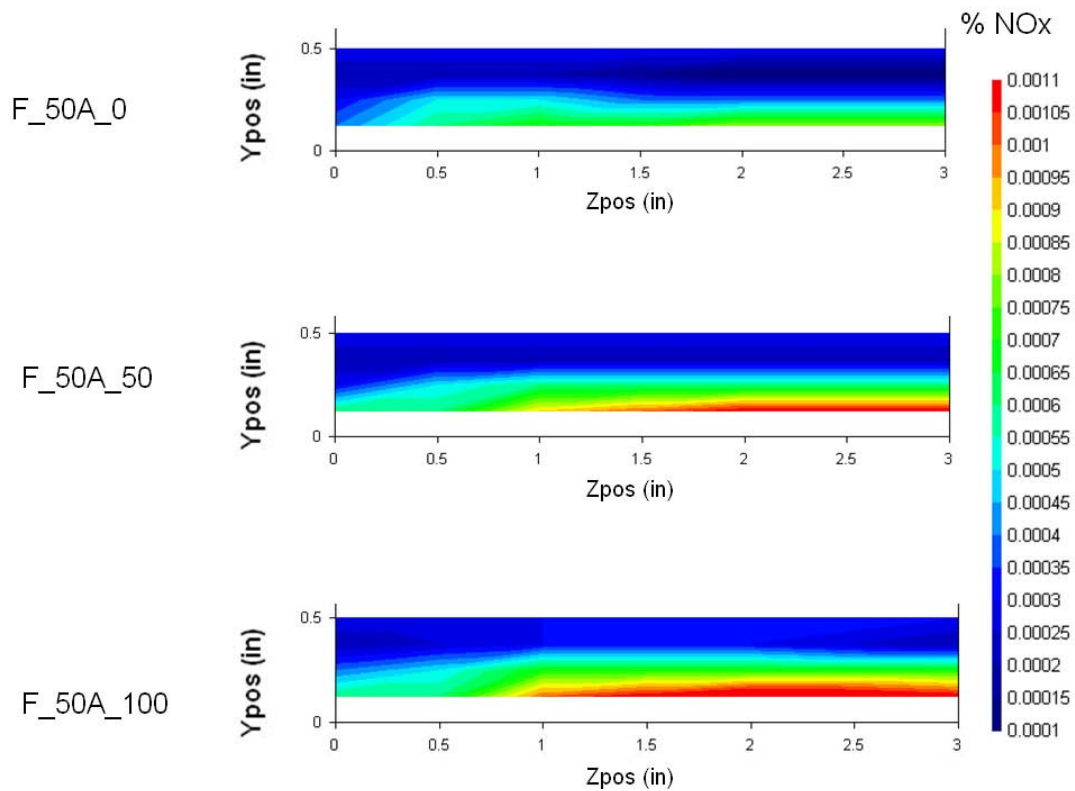

Figure 44. Nitrous oxide concentration behind cavity ramp with flow out of page for 50% ethylene. Fuel and air percentages are to the left (F_X A_Y, X = %ethylene Y = %air).

As with the lower fuel setting, NO_x production was low. Interestingly, NO_x production occurred on the same concentration scale for both fuel settings, indicating that an increase in fuel does not automatically ensure an increase in nitrous oxide production. The effect of adding an initial amount of air injection (from 0% to 30% for 32% ethylene injection, and from 0% to 50% for 50% ethylene injection) was greater with the 50% fuel loading than with the 32% fuel loading. Further air injection resulted in increased NO_x production, primarily in the core area of the combustion lobe. For 50% ethylene injection, the continuing increase in NO_x concentration with increasing air injection agrees with O_2 and C_xH_y concentration data (shown in Figures 40 and 43) and temperature data (shown in Figure 26) and indicates increased combustion.

Ramp Heating:

Since the material safety concerns often limited either test duration or the test grid resolution, and since the ability of materials to withstand high temperatures is of great interest currently, it is interesting to examine which of the fuel-air settings placed the greatest thermal load on the aft cavity ramp. This is shown in Table 8.

Table 8. Cavity ramp heating data.

Fuel-Air Setting	Peak Temp (°F)	Time to 900 °F (sec)
Baseline	552	N/A
F_32 A_0	1080	32
F_32 A_30	1074	30
F_32 A_70	1011	47
F_50 A_0	1077	23
F_50 A_50	942	44
F_50 A_100	887	60+

From Table 8 it is clear that the addition of air injection, particularly levels at or above 50%, results in substantial reductions in peak material temperature. Air injection also increases the time to reach the safety limit (1000 °F), as shown in the third column. What is noteworthy is that while energy spread into the free stream increases as air injection increases (see Figures 33 and 34), the cavity ramp material temperatures are lower (column 2 of Table 7). Thus not only can air injection be used as a combustion tuning mechanism that increases efficiency, but also for cooling the cavity.

V. Conclusions and Recommendations

Conclusions:

This research, in building on work done by Allen (2005), has demonstrated that cavity-based flameholders employing a direct fueling scheme are effective means of spreading combustive energy into the free stream flow of a supersonic combustor. The region of influence appears relatively small, with high temperature regions being contained within 0.5 in (approximately 20% of combustor cross-sectional area for the combustor setup used in this research) from the combustor floor.

Furthermore, the addition of direct air injection has been shown to be a highly flexible means of improving combustion throughout the cavity. Direct air injection serves to improve the fuel-air mixture within the cavity. By improving the fuel-air mixture in the cavity, higher fuel loading can be used without creating a cavity environment that is too fuel-rich to sustain efficient combustion.

Direct air injection improved combustive enthalpy release in all cases. For lower fuel loadings such as the 32% fuel injection level, the addition of air injection can increase enthalpy release to a level greater than a simple increase in fuel loading alone (50% fuel setting). The ability of direct air injection to reduce the amount of fuel wasted on inefficient combustion is a distinct benefit.

The addition of air injection within the cavity also functioned to cool the cavity's aft ramp. Significant decreases in peak ramp temperature reached over a given period of run time were seen as a result of air injection. The effect continued with additional air injection.

The addition of air injection leads to increases in total pressure losses. On a percentage- increase basis the total pressure losses tended to be greater than the gains in enthalpy. The ratio of percentage-increase in total pressure losses to enthalpy gain was reduced as fuel loading was increased. Further increases in fuel injection may lead to the percentage gain in enthalpy release outweighing the percentage increase in total pressure losses.

Recommendations for Further Research:

This initial research quantifying the performance of directly-fueled cavity-based flameholders augmented with direct air injection could be greatly enhanced with further work that researches a much wider array of fuel-air settings. This would allow a more complete picture regarding the behavior of aerothermodynamic properties as functions of fuel and air injection rates. Also, increasing the limits on fuel and air injection would serve to ascertain the limits of the direct fuel-air injected cavity. That is, one could determine just how much fuel and air can be injected and combusted within a given cavity geometry and volume. Furthermore, different cavity geometries and injection sites need to be investigated to determine if any one setup benefits more and loses less from direct air injection. The effect of increasing combustor backpressure also needs to be investigated, as lower flight Mach numbers will result in the shock train moving upstream of the cavity. The presence of the upstream shock train will most likely result in a region of high subsonic flow over the cavity, which may improve the ability of the cavity to spread combustion energy into the free stream flow.

In this research, all probing was done at a position 2.25 in downstream of the cavity flameholder. By using probes either made of more thermally resistant materials or that employ active cooling, measurements could be taken much closer to the cavity exit. Modifications in probe geometries would allow for data sampling closer to the tunnel floor in order to gain a more complete picture of the varied measurement distributions.

In order to conduct a more thorough gas mixture analysis, a different type of gas analyzer would be necessary. The ECOM-KL gas analyzer unit did not provide enough measurements to gain a complete picture of cavity emissions. Taking emissions data nearer to the cavity would reduce the influence of the free stream flow on measurements intended to represent emissions from the cavity itself.

Lastly, additional research needs to be conducted regarding scaling the cavity flameholder with increasing combustor size for full-scale implementation. The region of influence for this research was roughly 0.5 in from the combustor floor. While this distance makes up approximately 20% of the combustor height in this research, it is still a relatively small region of influence that must be increased in a full-sized combustor. One possible investigation would be to examine the effect of adding a strut or obstruction upstream of the cavity as a means of improving the energy spread into the free stream by the flameholder.

Appendix A

Reducing Combustion Time:

One method of reducing the ignition time of hydrocarbon fuels is to operate the combustor at a higher temperature. Deshaies et al. (1997) showed the relation of ignition delay to temperature, in that an increase in temperature typically leads to a reduction in ignition time. The relation between ignition delay and temperature is echoed by Maurice et al. (2000) for hydrocarbon fuels. They showed that the combustor entrance temperature imposed by the flight condition is typically half the temperature necessary to reduce the ignition delay time to 10% of the flow residence time. Simply increasing the temperature is not the solution to the task of reducing hydrocarbon ignition delay time. Deshaies et al. (1997) also demonstrated that raising the temperature without bound resulted in decreasing reductions in ignition delay time. Additionally, raising the temperature without bound introduces the same difficulties in selection of combustor materials discussed earlier.

Another method that has been undergoing extensive research is using the hydrocarbon fuel as a heat sink, as discussed by Maurice et al. (2000), to absorb heat flux from the engine, the flight vehicle skin, or both. This not only cools the vehicle-engine unit, but it imparts thermal energy into the fuel which allows the fuel to undergo thermal cracking, dehygrogenation, aromatic ring fracture, among others (Maurice et al., 2000). Endothermic fueling is beneficial because it acts almost as a pre-burner for the fuel. Endothermic fuels use waste heat from the aircraft or engine to partially react the fuel

before it is even injected into the combustor flow. Decomposing a larger hydrocarbon

fuel molecule such as kerosene down into smaller hydrocarbons noticeably reduces the

ignition delay time, as Colket and Spadaccini (2001) showed, with ethylene having

shorter ignition delay times than higher order hydrocarbons such as heptane, and heptane

having shorter ignition delay times than common fuels such as JP10. This process is not

without its drawbacks. The thermal decomposition process allows for unwanted deposits

forming within the fuel system, which will inevitably lead to system fouling and possibly

malfunction. Care must be taken to use these endothermic fuels in a way that draws as

much benefit as possible while doing the least amount of damage to the fuel system. To

accomplish this, further understanding needs to be gained in the chemical kinetics of

these endothermic processes.

Enhancing the Mixing Process:

The residence time of the core flow can be increased by disturbing it with an

obstruction, but this is undesirable because of the drag that would result from a large flow

path obstruction. Instead, much work has been done in improving fuel delivery and

mixing techniques. These will be discussed below, although a complete discussion of

every available mixing method is beyond the scope of this research.

It is important to establish the benefits and costs of each technique in order to arrive at an

optimal configuration.

Active Mixing:

Active mixing devices typically either use some form of active control, such as

with controllable actuators or pulsating jets, or they involve the use of an outside power

source such as with plasma torches or electromagnetic fields. There are numerous investigations into these methods in literature, but as this research involves the study of a passive mixing device, it is unnecessary to discuss all of them.

Passive Mixing:

Passive mixing in a general sense is a method that uses only the geometry of the flow enclosure and the fuel injection method to mix fuel and oxidizer. Some examples are parallel injection, strut injection, transverse injection, ramp injection, and the employment of cavity-based flameholders.

Parallel Wall Injection:

Parallel wall injection involves injecting fuel in a downstream direction parallel along the combustor sidewall. Parallel wall injection is a fuel delivery method that has the added benefit of cooling the combustor sidewalls. Parallel wall injection also has lower total pressure losses than those associated with strut injection, which will be mentioned later. Seiner et al. (1999) demonstrated that parallel injection provides for minimal pressure losses, as the core flow is not obstructed. One concern with wall injection comes from its difficulty in establishing combustion. Paull and Stalker (2000) showed that fuel injection parallel to the combustor wall caused the temperature near the wall to be cooler than what allows for self-ignition. Parallel injection also does not typically establish good combustion efficiency throughout the combustor, as it has poor mixing qualities at supersonic speeds.

Transverse Injection:

Transverse mixing generally refers to fuel injection methods with angles non-parallel to the free stream. There are variations on this theme ranging from simple changes in injection angle and orifice geometry, to adding swirl to the injection, and setting up sequential injectors to form a cascade injector. Port injection effectiveness can vary widely, as the variations mentioned above cause widely differing mixing effects.

The most basic style would be a completely transverse injection scheme, with the fuel flow normal to the free stream flow. Figure A1 is a diagram of the general flow field effects resulting from transverse injection.
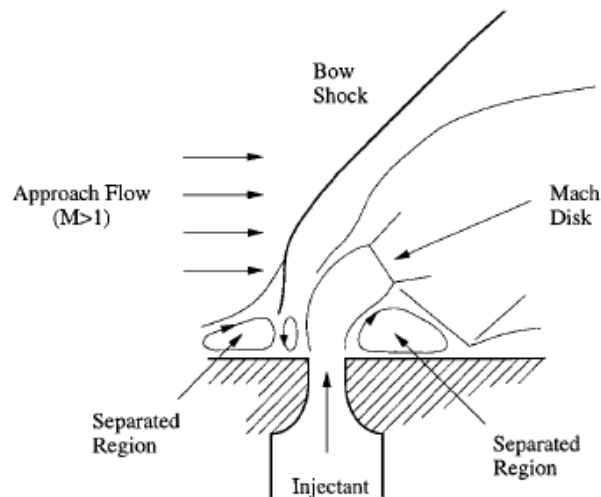

Figure A1. Flow field resulting from transverse fuel injection into a supersonic flow
(Gruber et al., 2000; used without permission).

As can be seen, a shockwave forms off the leading edge of the fuel injection port. Ben-Yakar and Hanson (1998) demonstrated that decreasing the angle between the injection axis and the free stream flow axis results in less penetration, but weaker shock formation.

Adding swirl to the injectant has been reported by Seiner et al. (1999) to increase the spread of the fuel plume laterally across the combustor section and has been shown to increase the amount of mixing within the shear layer. Gruber et al. (2000) showed that elliptical fuel injection ports can improve lateral spreading qualities of the fuel plume, while reducing the transverse spread of the same. Cascade injectors are a series of individual fuel injector ports aligned so as to create a fuel plume with more axial and transverse spread through the combustor. Siebenhaar et al. (1999) demonstrated that cascade injectors have shown noticeable improvements over a standard transverse injection setup, both in penetration and mixing.

Use of Flow Obstructions and Steps:

Strut injection, mentioned earlier, uses a physical obstruction protruding into the main flow to provide a shield against the main flow. Physical obstructions provide recirculation zones for fuel and air to mix and combust. Strut injectors can also function as a means to simply position the fuel injector farther into the main flow so as to allow the fuel plume to penetrate further into the main flow. Strut injectors typically provide good mixing qualities, but their use leads to significant total pressure losses. An example of a strut injector is the pylon injector, where a pyramidal obstruction is placed in front of a transverse fuel injection port. A generic form of injection behind an obstruction is shown below in Figure A2.
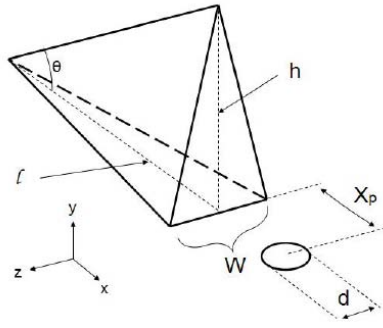
Figure A2. Pylon strut upstream (free stream direction is X-axis) of transverse injection port (Montes, 2005; used without permission).

Since the pylon is a flow path obstruction, shockwaves will be formed off its surfaces. Montes (2005) confirmed that shockwaves are formed off of the pylon. The presence of these added shockwaves will result in total pressure losses. However Montes (2005) clearly showed increased penetration height over the no-pylon transverse injection method. Whether the increased mixing efficiency offsets any losses from shock formation requires further research.

Step injectors shield the fuel injector from the high speed free stream flow without obstructing the free stream as much as a strut injector would. The step injector injects the fuel behind a step built into the combustor section. According to Kutschenreuter (2000), injecting fuel behind a step provides a recirculation zone that can serve as an ignition point and as a flameholder. It should be noted that there will be boundary layer separation at the step, but Kutschenreuter (2000) did not deem this problematic.

Ramp injection is similar to step injection, but also obstructs the main flow similar to a strut injector. Fuel is injected parallel to the wall out of the aft end of a raised ramp section in the combustor. Ramp injection is an attempt to gain some of the cycle

efficiency of parallel injection while at the same time achieving improved mixing
characteristics associated with steps or flow obstructions. Rogers et al. (1998) studied
ramp injectors in great depth. Figure A3 is an illustration of a ramp injector used in their
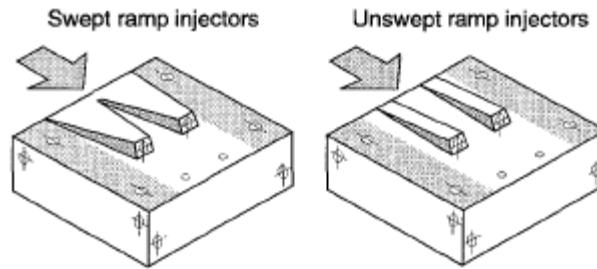study.

Figure A3. Ramp injector mixing setup (Rogers et al., 1998; used without permission).

There are different variations of ramp injectors, such as the swept and unswept versions
shown above. The presence of the ramp in a supersonic flow field creates both shock and
expansion waves. Seiner et al. (1999) theorized that these waves cause the density and
pressure gradients to be non-parallel to each other, resulting in vorticity induced by
baroclinic torque. The induced vorticity leads to an often observed lobe structure of the
fuel plume, as shown by Rogers et al. (1998). Ramp injectors can also be integrated into
a compression or expansion section within the combustor, as shown below in Figure A4.
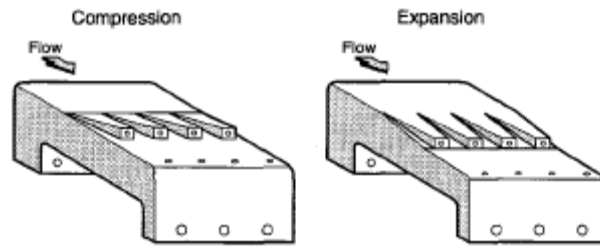
Figure A4. Ramp injectors in compression and expansion setup (Rogers et al., 1998; used without permission).

Rogers et al. (1998) showed that while both the standard ramp, swept or unswept (Figure A3), and the compression or expansion ramp injectors (Figure A4) provided combustion efficiencies somewhere between those of transverse injection (high end) and parallel injection (low end), the expansion ramp showed no autoignition capabilities, and poor flameholding ability.

Appendix B

Error Analysis:

The aerothermodynamic probing method and data reduction algorithm employed during this research were similar to those used by Fuller et al. (1998). They reported estimated uncertainties (within a 95% confidence interval) of the reduced data values as $\Delta M = \pm 1.7\%$, $\Delta P_t = \pm 2.8\%$, $\Delta P = \pm 2.8\%$, $\Delta \rho = \pm 3.0\%$, $\Delta u = \pm 1.3\%$, and $\Delta T = \pm 0.8\%$. Fuller et al. (1998) accounted for the mixture fractions of a binary gas in their data reduction, whereas this research assumed the flow the probes were exposed to consisted mostly of air alone. The uncertainties for the reduced quantities for this research may actually be lower, but the values used by Fuller et al. (1998) provide an established, and possibly conservative, estimation of error. The uncertainties of the computed enthalpy values are estimated to be $\Delta h = \pm 1.0\%$, and $\Delta(h/h_t) = \pm 2.5\%$. The uncertainty of the computed mass flux is Δmass flux $= \pm 3.3\%$. The mass flux was used in weighting the average enthalpy gain and total pressure loss for a given test run. Since the mass flux was used as a weighting factor, its uncertainty was disregarded in computing uncertainties of the mass flux average values of $\Delta P_t/P_t$ and $\Delta h/h$, which were found to be $\pm 2.8\%$ and $\pm 1.1\%$ respectively.

The other source of error for data reduction is the assumption of air alone for the composition of the flow measured by the probes. Previously it was argued that the flow measured by the probes was mostly air, on a mass flow basis. One can also see that if the flow composition is significantly different from air the variation in the specific heat ratio

is small. Table B1 below shows specific heat ratios computed for air alone (.21 O_2 + .79

N_2), a completely combusted stoichiometric ethylene-air reaction, a completely

combusted stoichiometric kerosene-air reaction (for comparison purposes), and for a flow

with species composition similar to the emissions data seen for the 50% fuel – 100% air

test run (which resulted in the greatest change from a mixture composition of air alone).

Specific heat ratios were calculated at 500 K and 800 K, since these were the low and

high temperatures, respectively, measured by the probes for reacting flow.

Table B1. Computed specific heat ratios for various gas mixtures in flow measured by probes.

Emissions Model	γ(500K)	γ(800K)	% Difference from Air	
			500K	800K
Air	1.37	1.35	N/A	N/A
Kerosene-Air	1.23	1.21	10.7	10
Ethylene-Air	1.31	1.29	4.5	4.5
Measured	1.38	1.35	0.4	0.2

The mixture compositions for the kerosene-air and ethylene-air reactions were computed

using the STANJAN equilibrium combustion code developed at the California Institute

of Technology. As shown is Table B1, the percentage difference in specific heat ratio for

flow consisting of the combustion products of an ethylene-air reaction is within 5% of the

specific heat ratio of air alone at both temperature extremes. The percentage difference

in the specific heat ratio for a flow with approximately the same gas composition as the

measured flow and the specific heat of air alone was within 1%. With the measured flow

gas composition closely resembling that of air alone, assuming air alone for gas

composition in the data reduction process is reasonable.

References

Allen, W.H., *Fuel-Air Injection Effects on Combustion in Cavity-Based Flameholders in a Supersonic Flow.* MS thesis, AFIT/GAE/ENY/05-M02. Graduate School of Engineering and Management, Air Force Institute of Technology, Wright-Patterson AFB OH, March 2005.

Ben-Yakar, A. and Hanson, R. K., "Cavity Flameholders for Ignition and Flame Stabilization in Scramjets: Review and Experimental Study," AIAA paper 98-3122, July 1998.

Colket III, M.B., and Spadaccini, L.J. "Scramjet Fuels Autoignition Study". *AIAA Journal of Propulsion and Power* Vol.17 No.2, 2001, pp. 315-323.

Deshaies, B., Figueira da Silva, L.F., and René-Corail, M. "Some Generic Problems Related to Combustion of Hydrogen and Air in Supersonic Flows", *IUTAM Symposium on Combustion in Supersonic Flows*, Kluwer Academic Publishers, Inc., 1997, Dordrecht, The Netherlands, pp. 15-42.

Dixon, D.R., Gruber, M.R., Jackson, T.A., Lin, K.-C., and Anthenien, R.A. "Structures of Angled Aerated-Liquid Jets in Mach 1.94 Supersonic Cross flow". *43rd AIAA Aerospace Sciences Meeting and Exhibit*, January 10-13 2005, Reno, NV.

Dooling, D. and Finckenor, M.M., "Material Selection Guidelines to Limit Atomic Oxygen Effects on Spacecraft Surfaces". NASA Technical Paper, NASA/TP—1999-209260, 1999.

Fuller, E. J., Thomas, R. H., and Schetz, J. A., ''Mixing Studies of Helium in Air at High Supersonic Speeds,'' *AIAA Journal*, Vol. 30, No. 9, 1992, pp. 2234– 2243.

Fuller, R.P., Wu, P-K, Nejad, A.S., Schetz, J.A. "Comparison of Physical and Aerodynamic Ramps as Fuel Injectors in Supersonic Flow". *AIAA Journal of Propulsion and Power*, Vol. 14, No. 2, 1998, pp. 135-145.

Gruber, M., Baurle,R., Mathur,T., and Hsu, K., "Fundamental Studies of Cavity-Based Flameholder Concepts for Supersonic Combustors", *AIAA Journal of Propulsion and Power*, Vol. 17, No. 1, 2001, pp. 146-153.

Gruber, M.R., Donbar, J.M., Carter, C.D. and Hsu, K-Y., "Mixing and Combustion Studies Using Cavity-Based Flameholders in Supersonic Flow," *AIAA Journal of Propulsion and Power* Vol. 20 No. 5, 2004, pp.769-778.

Gruber, M.R., Nejad, A.S., "Development of a Large-Scale Supersonic Combustion Research Facility," AIAA paper 94-0544, 32nd *Aerospace Sciences Meeting and Exhibit*, January 10-13, 1994, Reno, NV.

Gruber, M.R., Nejad, A.S., Chen, T.H., and Dutton, J.C., "Transverse Injection from Circular and Elliptic Nozzles into a Supersonic Crossflow". *AIAA Journal of Propulsion and Power*, Vol. 16, No. 3, 2000, pp. 449-457.

Kutschenreuter, P. "Supersonic Flow Combustors". Progress in Astronautics and Aeronautics V189: *Scramjet Propulsion*, Ed. E.T. Curran and S.N.B. Murthy. American Institute of Aeronautics and Astronautics, Inc. VA, 2000, pp 513-568.

Liepmann, H.W. and Roshko, A., *Elements of Gasdynamics.* John Wiley & Sons, Inc., New York, NY 1957.

Maurice, L., Edwards, T., and Griffiths, J. "Liquid Hydrocarbon Fuels for Hypersonic Combustion". Progress in Astronautics and Aeronautics V189: *Scramjet Propulsion,* Ed. E.T. Curran and S.N.B. Murthy. American Institute of Aeronautics and Astronautics, Inc. VA, 2000, pp 757-822.

Montes, D.R., King, P.I., Gruber, M.R., Carter, C.D., Hsu, K-Y., "Mixing Effects of Pylon-Aided Fuel Injection Located Upstream of a Flameholding Cavity in Supersonic Flow". AIAA paper 05-3913, *41st AIAA/ASME/SAE/ASEE Joint Propulsion Conference and Exhibit*, July 10-13, 2005, Tucson, AZ.

Nestler, D.E., Saydah, A.R., and Auxer,W.L., "Heat Transfer to Steps and Cavities in Hypersonic Turbulent Flow". AIAA paper 68-673, *Fluid and Plasma Dynamics Conference*, June 24-26, 1968, Los Angeles, CA.

Paull, A and Stalker, R.J. "Scramjet Testing in the T3 and T4 Hypersonic Impulse Facilities". Progress in Astronautics and Aeronautics V189: *Scramjet Propulsion*, Ed. E.T. Curran and S.N.B. Murthy. American Institute of Aeronautics and Astronautics, Inc. VA, 2000, pp 1-46.

Rich, B.R. and Janos, L. *Skunkworks*. New York: Little, Brown and Company, 1994.

Rogers, R.C., Capriotti, D.P., and Guy, R.W., "Experimental Supersonic Combustion Research at NASA Langley". AIAA Paper 98-2506, *20th Advanced Measurement and Ground Testing Technology Conference*, June 15-18, 1998, Albuquerque, NM.

Seiner, J.M., Dash, S.M., and Kenzakowski, D.C., "Historical Survey on Enhanced Mixing in Scramjet Engines". *9th International Space Planes and Hypersonic Systems and Technologies Conference and 3rd Weakly Ionized Gases Workshop*, November 1-5, 1999, Norfolk, VA.

Siebenhaar, A., Bulman, M., Norris, R., and Thompson, M., "Development and Testing of the Aerojet Strutjet Combustor" AIAA paper 99-4868, *9th International Space Planes and Hypersonic Systems and Technologies Conference*, November 1-5, 1999, Norfolk, VA.

Weber, R.J. and MacKay, J.S. "An Analysis of Ramjet Engines Using Supersonic Combustion". NACA Technical Note 4386, 1958.

Vita

  In May of 2000, Scott G. Edens graduated from Rochester High School in Rochester, Illinois. Upon graduating high school he went on to pursue a Bachelor of Science degree in Aerospace Engineering at the University of Illinois. After finishing his undergraduate work in May of 2004, he began graduate studies towards a Master of Science degree in Aeronautical Engineering at the Air Force Institute of Technology. Upon graduation he will begin employment with General Electric Aircraft Engines in Evendale Ohio.

1. REPORT DATE (DD-MM-YYYY) 22-12-2005	2. REPORT TYPE **Master's Thesis**	3. DATES COVERED (From – To) 10/2004 - 12/2005

4. TITLE AND SUBTITLE	5a. CONTRACT NUMBER
Performance Measurements of Direct Air Injection in a Cavity-Based Flameholder for a Supersonic Combustor	5b. GRANT NUMBER
	5c. PROGRAM ELEMENT NUMBER
6. AUTHOR(S) Edens, Scott G.	5d. PROJECT NUMBER
	5e. TASK NUMBER
	5f. WORK UNIT NUMBER

7. PERFORMING ORGANIZATION NAMES(S) AND ADDRESS(S) Air Force Institute of Technology Graduate School of Engineering and Management (AFIT/ENY) 2950 Hobson Way WPAFB OH 45433-7765	8. PERFORMING ORGANIZATION REPORT NUMBER AFIT/GAE/ENY/06-02

9. SPONSORING/MONITORING AGENCY NAME(S) AND ADDRESS(ES) Air Force Research Lab Propulsion Directorate (AFRL/PRAS) 1950 Fifth Street Wright-Patterson AFB, Ohio 45433 DSN 785-7350	10. SPONSOR/MONITOR'S ACRONYM(S)
	11. SPONSOR/MONITOR'S REPORT NUMBER(S)

12. DISTRIBUTION/AVAILABILITY STATEMENT
APPROVED FOR PUBLIC RELEASE; DISTRIBUTION UNLIMITED.

13. SUPPLEMENTARY NOTES

14. ABSTRACT
For several years the Air Force Research Lab Propulsion Directorate has been studying the difficulties in fueling supersonic combustion ramjet engines with hydrocarbon based fuels. Recent investigations have focused on the use of direct air injection into a directly-fueled cavity-based flameholder. Direct air injection has been shown qualitatively to be a valuable tool for improving cavity combustion. Little quantitative data is available that characterizes the performance of cavity-based flameholders. The objective of this research was to quantitatively determine the specific advantages and disadvantages of the direct air injection scheme. This was accomplished via intrusive probing into a supersonic free stream flow at an axial location behind the cavity flameholder. Pitot and static pressure, total temperature, and gas sampling measurements were taken and the corresponding values were processed to yield relevant engineering quantities. Data were taken over a range of fuel and air injection rates. Direct air injection resulted in increased combustion throughout the area of interest behind the cavity. Air injection increased the static temperature and pressure throughout the area of interest. Enthalpy spread into the free stream was also increased through the use of air injection. Total pressure losses increased as a result of the direct air injection scheme. The ratio of enthalpy increase to increase in total pressure losses increased with higher fuel flow rates, indicating that the direct air injection technique shows more promise for higher fuel loadings.

15. SUBJECT TERMS
Supersonic Combustion, Flameholding, Direct Injection, Cavity, Probe, Measurement, Scramjet

16. SECURITY CLASSIFICATION OF:			17. LIMITATION OF ABSTRACT	18. NUMBER OF PAGES	19a. NAME OF RESPONSIBLE PERSON Dr. Paul I. King (ENY)
a. REPORT U	U	U	UU	108	19b. TELEPHONE NUMBER (Include area code) 937-255-3636 x4628 paul.king@afit.edu